Distribution of IP_3-mediated calcium responses and their role in nuclear signalling in rat basolateral amygdala neurons

John M. Power and Pankaj Sah

Queensland Brain Institute, University of Queensland, St Lucia, Queensland 4072, Australia

Metabotropic receptor activation is important for learning, memory and synaptic plasticity in the amygdala and other brain regions. Synaptic stimulation of metabotropic receptors in basolateral amygdala (BLA) projection neurons evokes a focal rise in free Ca^{2+} in the dendrites that propagate as waves into the soma and nucleus. These Ca^{2+} waves initiate in the proximal dendrites and show limited propagation centrifugally away from the soma. In other cell types, Ca^{2+} waves have been shown to be mediated by either metabotropic glutamate receptor (mGluR) or muscarinic receptor (mAChR) activation. Here we show that mGluRs and mAChRs act cooperatively to release Ca^{2+} from inositol 1,4,5-trisphosphate (IP_3)-sensitive intracellular Ca^{2+} stores. Whereas action potentials (APs) alone were relatively ineffective in raising nuclear Ca^{2+}, their pairing with metabotropic receptor activation evoked an IP_3-receptor-mediated Ca^{2+}-induced Ca^{2+} release, raising nuclear Ca^{2+} into the micromolar range. Metabotropic-receptor-mediated Ca^{2+}-store release was highly compartmentalized. When coupled with metabotropic receptor stimulation, large robust Ca^{2+} rises and AP-induced amplification were observed in the soma, nucleus and sparsely spiny dendritic segments with metabotropic stimulation. In contrast, no significant amplification of the Ca^{2+} transient was detected in spine-dense high-order dendritic segments. Ca^{2+} rises evoked by photolytic uncaging of IP_3 showed the same distribution, suggesting that IP_3-sensitive Ca^{2+} stores are preferentially located in the soma and proximal dendrites. This distribution of metabotropic-mediated store release suggests that the neuromodulatory role of metabotropic receptor stimulation in BLA-dependent learning may result from enhanced nuclear signalling.

(Resubmitted 19 November 2006; accepted after revision 9 February 2007; first published online 15 February 2007)
Corresponding author P. Sah: Queensland Brain Institute, The University of Queensland, St Lucia, Queensland 4072, Australia. Email: pankaj.sah@uq.edu.au

The basolateral amygdala (BLA) is an important locus in assigning affective value to sensory stimuli. The cellular mechanism that underlies this association is thought to be long-term synaptic plasticity within the BLA (LeDoux, 2000; Davis & Whalen, 2001). It is generally believed that these changes that underlie emotional learning are largely due to NMDA-receptor-dependent synaptic plasticity. However, neurons in the amygdala also express a variety of metabotropic receptors (Sah *et al.* 2003) that have been implicated in BLA-dependent learning. Thus, activation of metabotropic glutamate receptors (mGluRs) within the BLA has been found to be necessary both for fear conditioning and for some forms of synaptic plasticity (Fendt & Schmid, 2002; Rodrigues *et al.* 2002). The BLA also receives a dense cholinergic innervation (Ben-Ari *et al.* 1977), with cholinergic activity in the BLA being thought to enhance consolidation of hippocampal-dependent memories that evoke an emotional response (Power *et al.* 2003). Blockade of muscarinic receptors (mAChRs) attenuates long-term potentiation in the amygdala (Watanabe *et al.* 1995) and impairs Pavlovian fear conditioning, as well as amygdala-dependent instrumental conditioning (McGaugh, 2004; Tinsley *et al.* 2004). However, while glutamatergic and cholinergic metabotropic receptors have been clearly implicated in BLA-dependent learning, the underlying cellular mechanisms for these actions are not well understood.

In BLA projection neurons, activation of either cholinergic or glutamatergic metabotropic receptors suppresses a number of K^+ conductances that control neuronal excitability (Washburn & Moises, 1992*b*; Womble & Moises, 1992, 1993, 1994; Yajeya *et al.* 1999). In addition, these receptors also stimulate the formation of inositol 1,4,5-trisphosphate (IP_3) which can release Ca^{2+} from intracellular stores (Berridge, 1998). In recent

 DOI: 10.1113/jphysiol.2006.125062

years, activation of metabotropic receptors linked to the generation of IP_3 has been shown to lead to release of Ca^{2+} from internal stores in a variety of neuronal cell types. This release can be focal, as in cerebellar Purkinje neuron spines (Finch & Augustine, 1998), or can propagate as waves through the dendritic tree as in hippocampal and cortical pyramidal neurons and midbrain dopamine neurons (Jaffe & Brown, 1994; Pozzo-Miller *et al.* 1996; Nakamura *et al.* 1999; Kapur *et al.* 2001; Power & Sah, 2002; Larkum *et al.* 2003; Morikawa *et al.* 2003). Of these, Ca^{2+} waves have only been described in detail in hippocampal and cortical pyramidal neurons (Ross *et al.* 2005). While the exact physiological role of these propagating Ca^{2+} rises is not known, release of Ca^{2+} from intracellular Ca^{2+} stores has been suggested to play a role in the induction of synaptic plasticity (Barbara, 2002; Fitzjohn & Collingridge, 2002), providing a possible link between synaptic activity and changes in gene transcription (Berridge, 1998). Consistent with this proposal, exogenous application of muscarinic agonists in hippocampal pyramidal neurons evokes Ca^{2+} waves that propagate from the dendritic tree and invade the nucleus (Nakamura *et al.* 1999; Kapur *et al.* 2001; Power & Sah, 2002; Larkum *et al.* 2003). Such rises in nuclear Ca^{2+} have been shown to activate CREB-mediated gene transcription (Dolmetsch *et al.* 1998; Li *et al.* 1998; Hardingham *et al.* 2001) in isolated cell systems. However, while dendritic Ca^{2+} waves can be evoked by repetitive synaptic stimulation (Jaffe & Brown, 1994; Pozzo-Miller *et al.* 1996; Nakamura *et al.* 1999; Kapur *et al.* 2001; Power & Sah, 2002; Larkum *et al.* 2003), synaptically evoked rises in nuclear Ca^{2+} have not been shown.

We have recently reported that synaptic stimulation of BLA projection neurons can evoke Ca^{2+} waves that initiate in the dendritic tree and propagate to the soma (Power & Sah, 2005). In the present study we examined the distribution of Ca^{2+} release evoked by metabotropic glutamate and muscarinic acetylcholine receptors and determined how these two systems interact to raise cytosolic Ca^{2+}. We show that Ca^{2+} waves can result from either muscarinic or metabotropic glutamate receptor activation and that coactivation of the two receptor types can lead to a superlinear amplification of the Ca^{2+} response. We also show that synaptically evoked Ca^{2+} waves can invade the nucleus. Furthermore, IP_3 generated during synaptic stimulation can interact synergistically with action potentials (APs) to amplify the nuclear Ca^{2+} response. This IP_3-mediated store release is restricted to the soma, nucleus and proximal dendrites, and is not observed in the distal spine-dense dendrites where the majority of excitatory synaptic contacts are made. This compartmentalization of IP_3 sensitive Ca^{2+} stores suggests a primary role of metabotropic-evoked Ca^{2+} store release in nuclear signalling.

Methods

Coronal brain slices (350–400 μm) were prepared using standard techniques (Power & Sah, 2002). Wistar rats (21–28 days old) were anaesthetized with halothane and decapitated. These procedures were in accordance with the guidelines of the Institutional Animal Ethics Committee of the University of Queensland. Slices were incubated at 33°C for 30 min and then maintained at room temperature in an artificial cerebral spinal fluid (ACSF) solution containing (mM) 119 NaCl, 2.5 KCl, 1.3 $MgCl_2$, 2.5 $CaCl_2$, 1.0 Na_2PO_4, 26.2 $NaHCO_3$, 11 glucose, equilibrated with 95% CO_2, 5% O_2. Slices were perfused with ACSF heated to 33°C, and whole-cell recordings were made from the soma of BLA neurons using infrared differential interference contrast videomicroscopy. Patch pipettes (2–5 MΩ) were filled with an internal solution containing (mM) 135 $KMeSO_4$, 8 NaCl, 10 Hepes, 2 Mg_2ATP, 0.3 Na_3GTP, 0.1 spermine (pH 7.3 with KOH, osmolarity 280–290 mosmol l^{-1}) and one of the following Ca^{2+} indicators: 50–100 μM Oregon Green BAPTA-1, or 300 μM Fluo-5F (Molecular Probes). In some experiments, Alexa 594 (30 μM) was also added to the internal solution to allow imaging of the cell structure. Electrophysiological signals were amplified with either an Axopatch 1D or a Multiclamp 700A amplifier (Molecular Devices), filtered at 5 kHz and digitized at 20 kHz with an ITC-16 board (Instrutech), and controlled using Axograph (Axon Instruments). Synaptic stimuli were generated using either a DS2A (Digitimer) or an Isolator-11 (Axon Instruments) isolated stimulator. Electrophysiological data were analysed using Axograph. Whole-cell recordings were obtained from projection neurons in the basal nucleus of the BLA. Only cells that had resting potentials more negative than −55 mV, AP amplitudes >100 mV, and membrane resistances (R_m) >60 MΩ, were included in the data set.

Whole-field fluorescence measurements were made using a monochromator based imaging system, Polychrome II (TILL Photonics GmbH). Neurons were visualized using a BX50 microscope (Olympus) equipped with a 60× water immersion objective (NA 0.9; Olympus) and illuminated with 488 nm light. IP_3 was uncaged using a 2 ms stimulation from a pulsed xenon arc lamp (TILL Photonics GmbH) that illuminated the entire field of view. Light from both the monochromator and the flash were delivered to the BX50 microscope via a quartz light guide and a custom epifluorescence attachment provided by TILL Photonics, and then to the cells through the objective. Images were acquired with an interline transfer, cooled CCD camera (TILL Photonics GmbH) in which the scan lines were binned by two in both horizontal and vertical directions, giving a spatial resolution of 0.33 μm per pixel. Frames were collected at 25–33 Hz with a 10 ms exposure time. Images were analysed offline using Vision (TILL Photonics GmbH).

Two-photon and single-photon confocal fluorescence images were obtained using a Zeiss Axioskop 2FS with a 510 laser scanning head. The Axioskop was equipped with an argon laser for single photon illumination and either a Chameleon laser (Coherent Scientific) or a Verdi solid-state pump laser with a Mira 900-F femptosecond Ti:S pulsed laser (Coherent Scientific) for two-photon excitation. The excitation wavelengths were 488 nm for single-photon excitation and 810 nm for two-photon excitation. Fluorescence images were acquired in line-scan mode (50–200 Hz) at a resolution of 10–20 pixels μm^{-1}. When acquiring single-photon confocal data, the detector pinhole aperture was set to give an axial resolution of $<1.5\,\mu m$. Small segments (3–5 μm) of the line were selected over each subcellular region and the fluorescence over this segment was averaged. Measurements of somatic Ca^{2+} were taken from the extranuclear soma, closest to the dendrite where the wave initiated. Nuclear measurements were taken from the centre of the nucleus.

Kinetic sequences were constructed over time for each of the selected regions. Kinetic sequences were calculated as the relative change in fluorescence over baseline fluorescence ($\Delta F/F$). $\Delta F/F_t = (F_t - F_0)/(F_0 - B)$ where F_t is the fluorescence at time t, F_0 is the average baseline fluorescence prior to the stimulus, and B is the background fluorescence measured in an adjacent extracellular region. In some two-photon experiments, Ca^{2+} indicators were coloaded with the marker dye Alexa 594 (30 μM) which is also excited at 810 nM but fluoresces red. The emitted light was split with a dichroic (DT560), bandpass filtered (green channel, 500–560 nm; red channel, 575–640 nM), and detected with separate non-descanned detectors. In these instances, kinetic sequences were calculated as the change in green fluorescence normalized to the red fluorescence, $\Delta G/R_t$.

Fluorescence kinetic sequences were analysed offline using custom software. Measurements for each region of interest included peak amplitude, peak latency, area of the Ca^{2+} response integrated over time, half-width, response onset latency, and rise-time. The onset of the response was calculated as the time point at which the response exceeded 3 standard deviations above the baseline period. The rise-time was calculated as the time taken to rise from 10% to 90% of the peak response. The wave propagation speed was measured as the time for propagation of the wave-front a distance of 10 μm along the dendrite. To measure Ca^{2+}-induced Ca^{2+} release at IP_3 receptors (IP_3-CICR), the peak and integrated area of the AP-evoked Ca^{2+} response in the presence of agonist were normalized to the AP-evoked responses without agonist for each region of interest. All data are presented as means ± S.E.M. unless otherwise stated. Statistical comparisons made using a paired Student's *t* test or ANOVA and Fisher's PLSD *post hoc* tests as appropriate.

In some cases the Ca^{2+} concentration was estimated using methods published by Maravall *et al.* (2000). To estimate Ca^{2+} changes ($\Delta[Ca^{2+}]_i$), and resting Ca^{2+} ($[Ca^{2+}]_{rest}$), we used the high-affinity indicator Oregon Green BAPTA-1 and the following formula:

$$\Delta[Ca^{2+}] = K_D \frac{F_{max}}{F_0}\left(1 - R_f^{-1}\right)\frac{\Delta F}{(\Delta F_{max} - \Delta F)\Delta F_{max}}$$

where R_f and K_D are the dynamic range and dissociation constant of the indicator, with $R_f = 5.7$ and $K_D = 210$ nM for Oregon Green BAPTA-1 (Maravall *et al.* 2000). Estimates of F_{max} and ΔF_{max} were obtained by measuring the amplitude of a saturating fluorescence plateau evoked by a prolonged high-frequency train of APs (100 Hz).

In some instances we also estimated the large Ca^{2+} amplitudes with the moderate affinity fluo-5F ($K_D \sim 2\,\mu$M) using the following formula (Yasuda *et al.* 2004):

$$[Ca^{2+}]_i = K_D\{(G/R) - (G/R)_{min}\}/\{(G/R)_{max} - (G/R)\}$$

On rare occasions the peak fluorescence signal was well beyond the linear range of the indicator and quite unreliable. To minimize the effects of these error prone values, estimates of peak Ca^{2+} were capped at 10 μM.

Low molecular weight heparin (500 $\mu g\,ml^{-1}$; Sigma) and *myo*-inositol 1,4,5-trisphosphate caged IP_3 (25–100 μM; Molecular Probes) were added to the internal solution as required. Acetylcholine, muscarine, carbachol, glutamate, and (1*S*,3*R*)-1-aminocyclopentane-1,3-dicarboxylic acid (t-ACPD) were applied either by focal pressure application (2–100 μM in ACSF) through a patch pipette using a picospritzer (10–30 p.s.i. (69–207 kPa), 50–500 ms; Parker Hannifin Fairfield, NJ, USA) or via iontophoresis. For iontophoretic application, current was delivered using the Multiclamp 700A amplifier and we adjusted the pH of acetylcholine (ACh) and t-ACPD to 4 and 8, respectively. ACh (10–50 mM) and muscarine (5 mM) were applied with a 10–50 nA ejection current with a −10 nA retention current. t-ACPD (2 mM) was applied with a −50 nA ejection current and a 10 nA retention current. All other drugs were bath applied. Cyclopiazonic acid (CPA), 1,2,3,4-tetrahydro-6-nitro-2,3-dioxo-benzo[f] quinoxaline-7-sulphonamide (NBQX), and 6-cyano-7-nitroquinoxaline-2,3-dione (CNQX) were prepared as stock solutions in DMSO, and diluted in ACSF when required. NBQX and 2-amino-5-phosphonovaleric acid (APV) were purchased from RBI. t-ACPD was purchased from Tocris. Tetrodotoxin (TTX) was purchased from Alomone Laboratories. All other drugs were obtained from Sigma.

The dendritic arborization of BLA projection neurons has no readily discernable orientation, so there was an

inherent bias in the selection of dendrites. In whole-field fluorescence imaging experiments there was a strong bias toward large apical-like dendrites. Confocal images were restricted to the first 150 μm of the dendritic tree. Imaged dendrites were located near the surface of the slice (<70 μm). *z*-Stacks were constructed to measure morphological features such as dendrite diameter, distance from soma, distance from the iontophoretic electrode and spine density. Spine density was estimated by making two dimensional projections from *z*-stacks and counting the number of spine protrusions visible over a 10 μm dendritic segment. While these measurements are likely to underestimate the actual spine density, there was a clear difference between spine-sparse and spine-dense dendritic segments. We defined branch order solely based on the branch points, with primary branches being between the soma and first branch point, secondary branches between the second and third branch point, and higher order branches being 2–3 branch points removed from the soma.

Results

Synaptic stimulation raises nuclear Ca^{2+}

Whole-cell patch-clamp recordings and fluorescence images were made from projection neurons within the basal division of the BLA. These neurons had a resting membrane potential of -66.0 ± 4.7 mV ($n = 195$; mean ± S.D.). Neurons in the basal nucleus receive glutamatergic input primarily from the cortex, hippocampus and lateral amygdala (Sah *et al.* 2003). To evoke Ca^{2+} waves, bipolar stimulating electrodes were placed either in the external capsule (EC), to preferentially activate cortical and hippocampal afferents, in the lateral amygdala (LA) to preferentially stimulate afferents from the LA, or locally with in the basal nucleus (B) to activate all afferent pathways. Neurons in the basal nucleus also receive extensive cholinergic innervation from the basal forebrain (Nagai *et al.* 1982; Mesulam *et al.* 1983; Carlsen *et al.* 1985) which traverses through the EC (Ichikawa & Hirata, 1986). EC stimulation has been shown to activate cholingeric afferents on BLA projection neurons (Washburn & Moises, 1992*b*; Womble & Moises, 1993). Unlike the hippocampus and cortex, the basolateral amygdala is not a layered structure and the dendritic trees of its neurons do not have any clear organization. Thus, neither the arborization patterns of these inputs nor the subcellular distribution of mAChRs or mGluRs on these neurons is known. Results from the lateral amygdala suggest that glutamatergic inputs to projection neurons may be dispersed throughout the dendritic tree (Humeau *et al.* 2005).

Using whole-field imaging and the Ca^{2+} indicator Oregon Green BAPTA-1 (50 μM) we found that Ca^{2+} waves could be evoked by tetanic stimulation (33–100 Hz, 0.1–2 s) at all stimulator locations. Ca^{2+} waves evoked by different stimulating electrode positions were indistinguishable. In each instance, Ca^{2+} waves began as a focal increase in the proximal dendrite (15–50 μm from the soma; EC, 21 ± 7 μm; LA, 33 ± 8 μm; B, 30 ± 5 μm) 300–1200 ms after the first stimulus and propagated toward the soma (Fig. 1*B* and *C*). A limited back propagation of the Ca^{2+} wave was also observed (see also Power & Sah, 2005). Similar to observations in CA1 pyramidal neurons (Nakamura *et al.* 2002), the wave initiation site tended to be near the first branch point. In 9 of 11 neurons, where both the wave initiation site and cell morphology were determined, Ca^{2+} waves initiated within 2 μm of the first or second branch point. On some occasions, synaptic stimulation evoked waves that propagated simultaneously from multiple dendrites (Fig. 1*D*). The propagation speed of the wave front along the dendrite varied considerably between neurons (median 95 μm s^{-1}; range 32–333 μm s^{-1}; $n = 14$).

Ca^{2+} waves were not observed to single synaptic stimuli, but could be evoked by as little as five stimuli (50 Hz), although 30–100 stimuli were more commonly used. APs were not required for wave generation as robust Ca^{2+} waves could be evoked by subthreshold summating synaptic potentials (Fig. 1). In these neurons, the amplitude of the evoked EPSP varied between 8.0 and 21.8 mV (mean 13.4 mV; $n = 8$). Wave generation did not require membrane depolarization or ionotropic glutamate receptors as waves could be evoked in voltage clamp ($n = 29$) and in the presence of NMDA and AMPA receptor antagonists ($n = 22$). As previously described, waves were more readily and repetitively evoked when Ca^{2+} stores were primed by subthreshold depolarizations (1–3 min), which activate low-threshold voltage-dependent Ca^{2+} channels, or by APs trains (Power & Sah, 2005). To minimize problems arising from voltage-dependent processes and store depletion, waves were typically evoked at 3–5 min intervals under voltage-clamp conditions (holding potential −50 to −55 mV) in the presence of NMDA and AMPA receptor antagonists.

Wave propagation was dependent on stimulus intensity such that near the threshold for wave generation, the Ca^{2+} rise was restricted to a local dendritic region (Fig. 1*E*, low stim); higher stimulus intensities resulted in more robust waves which propagated further (Fig. 1*E*, high stim). Increasing either the stimulus intensity (40–45 V DS2A stimulator, 500–700 μA Isolator-11 stimulator) or the number of stimuli also augmented the peak Ca^{2+} rise in the soma (0.37 ± 0.20 *versus* 1.16 ± 0.28 $\Delta F/F$; $n = 6$; $P < 0.05$) as well as the integrated area of the Ca^{2+} transient in the soma (0.32 ± 0.13 *versus* 2.32 ± 0.88 $\Delta F/F$ σ; $n = 5$; $P < 0.05$) and the proximal dendrite (0.67 ± 0.20 *versus* 1.46 ± 0.42 $\Delta F/F$ σ; $n = 6$; $P < 0.05$). While Ca^{2+} waves clearly invaded the soma, the Ca^{2+} rise was smaller in amplitude, and had a slower time course in the soma as compared to the

dendrite. Thus, with Oregon Green BAPTA-1 (50 μM), peak amplitude was $1.35 \pm 0.25\ \Delta F/F$ in the proximal dendrite as compared with $0.87 \pm 0.16\ \Delta F/F$ in the extranuclear soma ($P < 0.05$). The time-to-peak and half-width of the Ca^{2+} transient were 275 ± 34 and 515 ± 60 ms in the dendrite, significantly ($P < 0.01$) faster than in the extranuclear soma (471 ± 34 and 1059 ± 158 ms, respectively; $n = 22$).

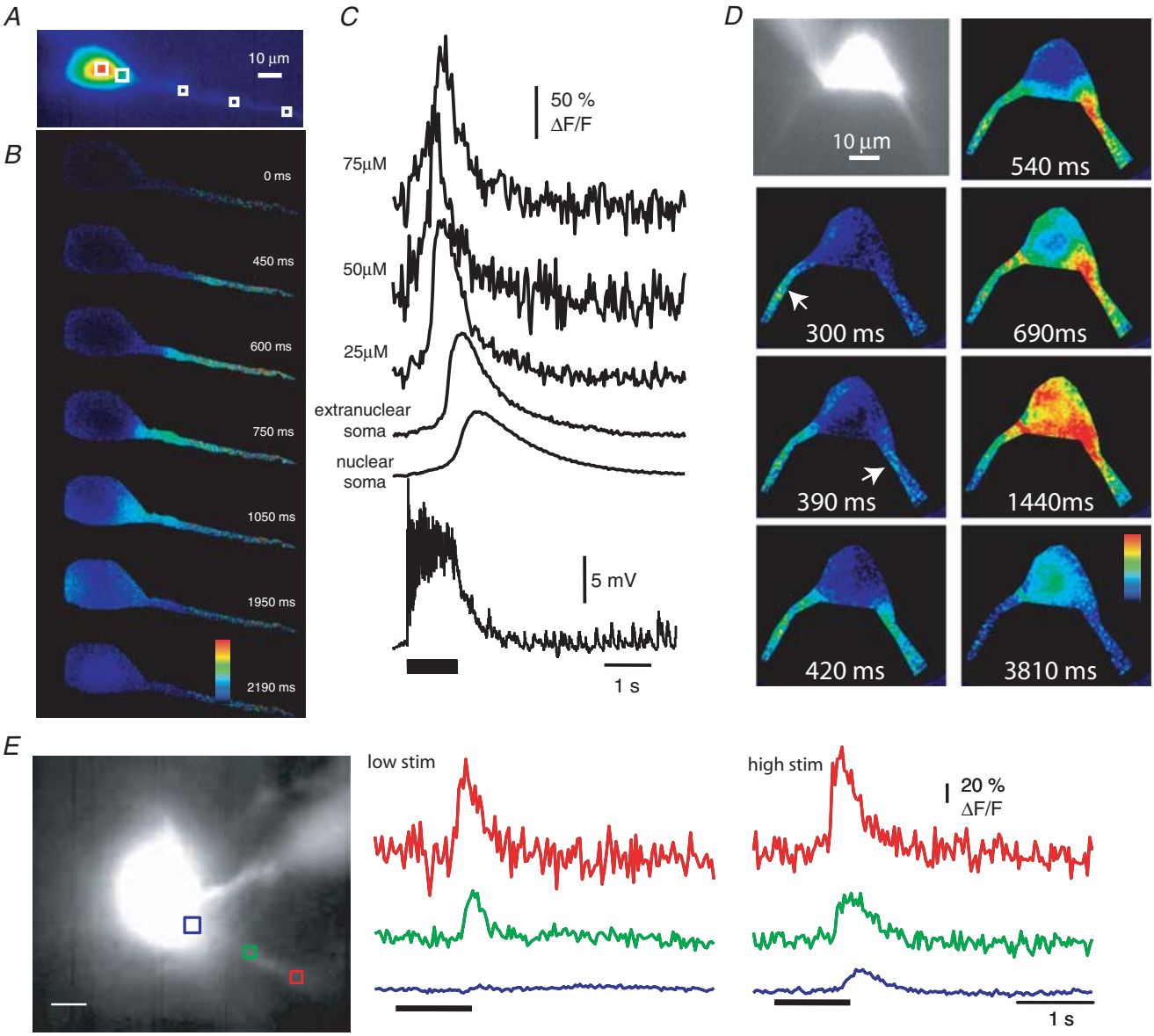

Figure 1. Synaptic stimulation evokes Ca^{2+} waves
A, fluorescence image of a cell loaded with 50 μM Oregon Green BAPTA-1. *B*, selected pseudo-colour frames ($\Delta F/F$) are shown at the indicated times after stimulation (50 Hz, 1 s) of the external capsule. *C*, rises in Ca^{2+}, plotted as $\Delta F/F$ measured at the extranuclear soma, nuclear soma and different distances from the soma (μm). The voltage response is shown beneath the $\Delta F/F$ plots. Resting membrane potential was −63 mV and no receptor or channel blockers are present in this example. Note that summating synaptic potentials remain subthreshold during the train. *D*, fluorescence image of a neuron loaded with Oregon Green BAPTA-1 with two primary dendrites visible. Pseudo-colour frames ($\Delta F/F$), taken at the indicated times after stimulation (100 Hz, 1 s) of the basal nucleus in the presence of 6-cyano-7-nitroquinoxaline-2,3-dione (CNQX; 20 μM) and 2-amino-5-phosphonovaleric acid (D-APV; 60 μM) under voltage-clamp conditions (V_m −70 mV). Ca^{2+} waves are observed emanating from two different dendrites, each propagating toward the soma. Arrows indicate the initiation point of the dendritic waves. *E*, Ca^{2+} waves evoked by tetanic stimulation (100 Hz, 1 s) of the external capsule in the presence of kynurenic acid (2 mM) under voltage clamp (V_m −70 mV). With low-intensity stimulation (40 V, 100 μs; low stim), Ca^{2+} rises are restricted to the dendrite (red and green). With higher stimulus intensity (45 V, 100 μs; high stim), waves propagate into the soma (blue). A fluorescence image of a neuron loaded with Oregon Green BAPTA-1 together with the selected regions of interest is shown on the left. Scale bar, 10 μm.

Whole-field imaging cannot separate signals arising from Ca^{2+} rises in extranuclear cytosolic regions from those arising within the nucleus. We therefore examined whether Ca^{2+} waves invade the nucleus using confocal imaging using the moderate affinity Ca^{2+} indicator Fluo-5F (K_D 2 μM) along with the Ca^{2+}-insensitive fluorophore Alexa 594. With confocal imaging, the nucleus appears as an area of brighter fluorescence of the red marker dye Alexa 594 (Fig. 2*A*). This difference in fluorescence intensity is most likely due to differences

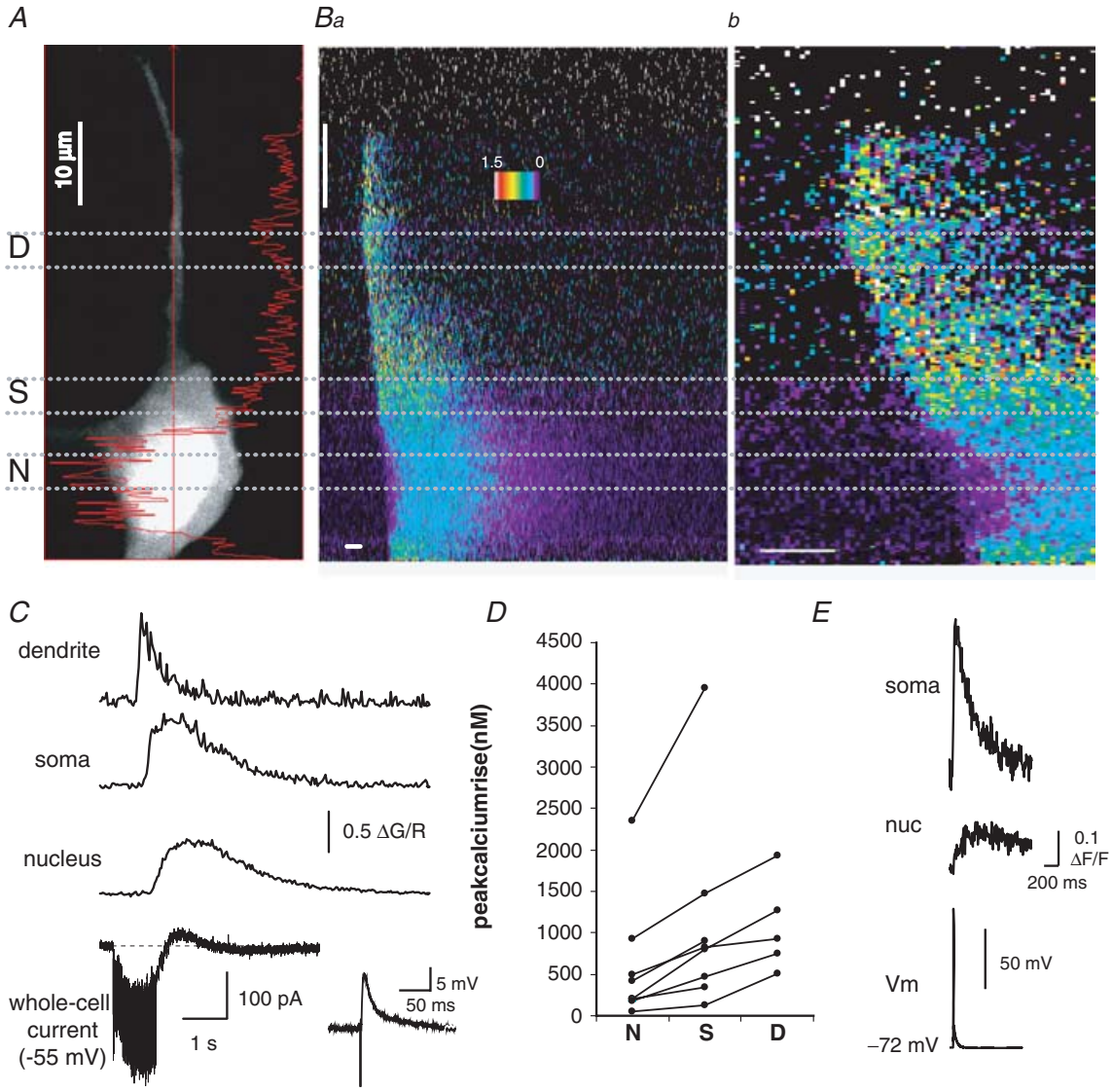

Figure 2. Synaptically evoked Ca^{2+} waves invade the nucleus
A, red fluorescence two-photon image for a basolateral amygdala (BLA) projection neuron loaded with the Fluo-5F (300 μM; K_D ~2 μM) and Alexa 594 (30 μM). The straight red line indicates the location of the scan line. Nuclear (N) somatic (S) and dendritic (D) segments are indicated by dashed lines. *B*, local synaptic stimulation (50 Hz, 1 s) causes a rise in Ca^{2+} in the dendrite, soma and nucleus. The fluorescence response along the scan line over time, plotted as $\Delta G/R$ on a pseudocoloured scale, is shown in *a* and on an expanded time scale in *b*. Horizontal scale bars, 250 ms; vertical scale bar, 10 μm. *C*, the Ca^{2+} response, plotted as $\Delta G/R$, is shown for the nucleus, soma, and dendrite in response to synaptic stimulation (50 Hz, 1 s). The whole-cell current (holding potential −55 mV) is shown below the Ca^{2+} response. The inset to the right of the current trace shows the voltage response to a single synaptic stimulation. *D*, summary data plotting the peak amplitude of synaptically activated Ca^{2+} waves, in the nucleus (N), soma (S) and proximal dendrite (D), 10–15 μm from the soma. Lines connect data from the same neuron. Data in *A–D* were acquired using moderate-affinity Fluo-5F. Waves that did not propagate to the somatic border are not included in *D*. *E*, fluorescence response, plotted as $\Delta F/F$, to a single AP in the nucleus and soma for a neuron loaded with Oregon Green BAPTA-1 (50 μM); note the slow kinetics of the nuclear Ca^{2+} signal.

in free intracellular space, as there is a relative lack of organelles in the nucleus, resulting in larger free intracellular volume per sampled volume and thus a brighter fluorescence signal in the nucleus for both the Ca^{2+} indicator and the marker dye (Connor, 1993). The two- to threefold difference in Alexa 594 fluorescence between the nucleus and cytoplasm that we observed corresponds well to published differences in freely diffusible space between the two compartments (Horowitz & Moore, 1974). Confocal imaging confirms (Fig. 2*B* and *C*) synaptically evoked Ca^{2+} waves can invade the nucleus. Furthermore, as can be seen in Fig. 2*C*, under voltage-clamp conditions synaptic stimulation (50 Hz, 1 s) generated an inward current due to summating EPSCs that do not reach threshold. Similar to results obtained using whole-field imaging, the amplitude of the Ca^{2+} wave varied between neuronal compartments (Fig. 2*D*) with the dendrite showing the greatest amplitude ($P < 0.05$, dend *versus* soma; $P < 0.001$, dend *versus* nucleus; $n = 5$). Compared with the extranuclear soma, the rise in nuclear Ca^{2+} was smaller in amplitude (0.40 ± 0.14 *versus* 0.61 ± 0.15 $\Delta G/R$, $P < 0.001$) and had a slower time course with the rise time and half-width in the nucleus being 1059 ± 110 and 1770 ± 322 ms as compared with 659 ± 115 ms ($P < 0.05$) and 860 ± 322 ms ($P < 0.001$), respectively, in the extranuclear soma. Ca^{2+} transients evoked by APs that open voltage-dependent Ca^{2+} channels in the plasmalemma showed similar slow kinetics in the nucleus (Fig. 2*E*). It was notable that the rise in nuclear Ca^{2+} following influx during single (Fig. 2*E*) or brief trains of APs was markedly smaller than that seen during invasion by a Ca^{2+} wave. We estimate (see Methods) that a single AP raises free Ca^{2+} by 70 ± 20 nM in the extranuclear soma and 14 ± 2 nM in the nucleus (estimated by evoking a single AP and the indicator Oregon Green BAPTA-1; $n = 6$). In contrast, synaptically evoked Ca^{2+} waves were able to raise Ca^{2+} concentration in the soma and nucleus by several hundred nanomoles (Fig. 2*D*, Fluo-5F; similar estimates were obtained in neurons loaded with Oregon Green BAPTA-1). The smaller amplitude and slower kinetics of the nuclear Ca^{2+} signal are consistent with diffusion of Ca^{2+} from the cytosol into the nucleus due to the slight diffusional barrier presented by the nuclear pores in the nuclear membrane (O'Malley, 1994).

These results show that repetitive synaptic stimulation raises cytosolic Ca^{2+} in the dendritic tree. This propagates as a wave to the soma and can raise nuclear Ca^{2+} to levels that are substantially higher than that achieved following APs. There has been some controversy regarding the measurement of nucleoplasmic Ca^{2+} (Bootman *et al.* 2002*a*), with it being suggested that under certain circumstances standing Ca^{2+} gradients between the nucleus and cytoplasm may exist, leading to differences in resting Ca^{2+} (Himpens *et al.* 1994; Bootman *et al.* 2002*a*). If resting Ca^{2+} in the nucleoplasm was substantially higher than in the cytosol, measurements of Ca^{2+} using $\Delta F/F$ may be prone to errors. In addition, biochemical differences between nuclear and cytoplasmic environments have been suggested to alter the behaviour of the TILL Photonics indicator, shifting the K_D of the indicator or quantum efficiency (O'Malley, 1994). However, we see no evidence for a resting Ca^{2+} gradient in BLA neurons. At rest, the ratio of Oregon Green BAPTA-1 to Alexa 594 fluorescence does not differ between compartments ($n = 7$; paired t test $P = 0.79$). Furthermore, using high-frequency trains of APs to saturate the fluorescence signal, we found no differences in the maximal fluorescence (G_{max}/G_0) between the two compartments (see Supplemental Fig. 1). When the green fluorescence signal is normalized to the red marker dye fluorescence we find that the saturation level (G_{max}/R) does not differ between compartments regardless of indicator (Oregon Green BAPTA-1 or Fluo 5F). These results indicate that the quantum efficiency of the indicators does not differ between compartments. We cannot rule out the possibility that differences in the K_D of the indicator are masking differences in resting Ca^{2+}, and that our estimation of the Ca^{2+} concentration in the nucleus may therefore be subject to some error. However, our finding that Ca^{2+} waves invade the nucleus, and are substantially more effective than APs at raising nuclear Ca^{2+} is insensitive to differences in indicator behaviour between the nucleus and cytoplasm.

Cooperative action of mAChRs and mGluRs in wave generation

In pyramidal neurons, activation of either metabotropic glutamate receptors (mGluRs; Nakamura *et al.* 1999; Larkum *et al.* 2003) or muscarinic acetylcholine receptors (mAChRs; Power & Sah, 2002) can generate Ca^{2+} waves. Both mGluR5 metabotropic glutamate receptors (Rodrigues *et al.* 2002) and mAChRs (Mash & Potter, 1986) are present at high concentrations in the BLA. As the location of our stimulating electrodes will activate both glutamatergic and cholinergic afferents to BLA neurons, we tested for the involvement of these systems in wave generation. Waves were evoked at 3–5 min intervals under voltage-clamp conditions (holding potential -50 to -55 mV) in the presence of the ionotropic receptor blockers APV and CNQX. After obtaining a stable baseline, we bath-applied saturating concentrations of either the mAChR antagonist atropine or the mGluR5 antagonist 6-Methyl-2-(phenylethynyl) pyridine (MPEP) (Gasparini *et al.* 1999). Atropine (1 μM) reduced the peak Ca^{2+} response by $81 \pm 10\%$ in the soma ($P < 0.01$) and $80 \pm 16\%$ in the proximal dendrite (Fig. 3*B*; $n = 5$; $P < 0.05$). MPEP (10 μM) reduced the Ca^{2+} response by $65 \pm 17\%$ in the soma ($n = 6$; $P < 0.05$) and $40 \pm 20\%$ in the proximal dendrite (Fig. 3*C*). Following application of either atropine or MPEP, there was no change in

the initiation point of the Ca^{2+} wave. However, the onset of the Ca^{2+} wave was delayed by 34 ± 7 ms ($n = 5$; $P < 0.01$; atropine 1, MPEP 4). There was no detectable rise in Ca^{2+} in the presence of both antagonists ($n = 3$). Consistent with a role of both mAChRs and mGluRs in the synaptic generation of Ca^{2+} waves, robust Ca^{2+} waves were reliably evoked with focal pressure application of either muscarine (5–20 μM) or t-ACPD (5–20 μM), or with iontophoretic application of ACh (10–50 mM), muscarine (5 mM) or t-ACPD (2 mM) (Fig. 3*C*). Similar to synaptically evoked waves, Ca^{2+} transients evoked by exogenously applied agonists propagated along the

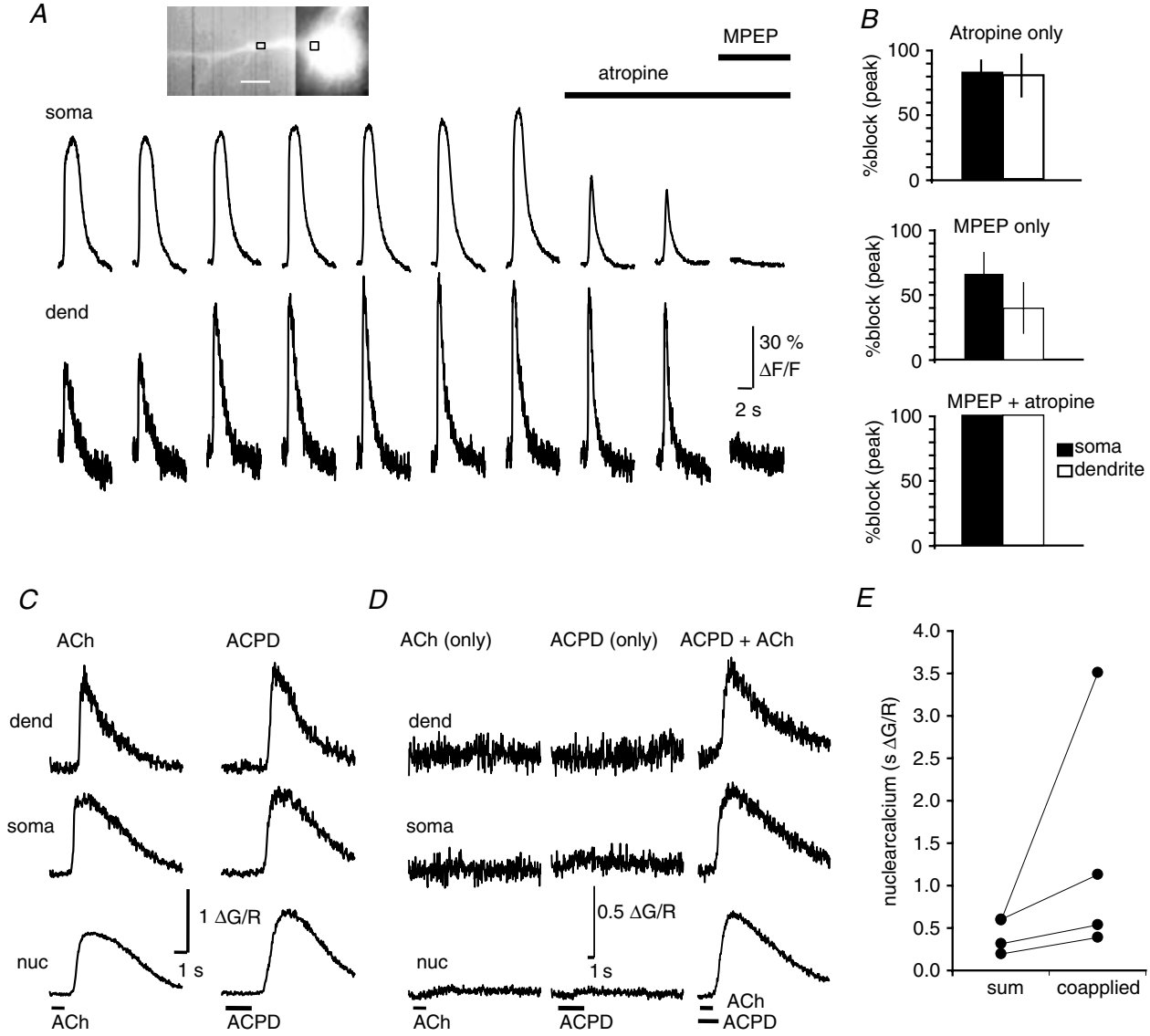

Figure 3. Ca^{2+} waves are mediated by metabotropic receptor activation
A, Ca^{2+} waves repetitively evoked once every 5 min by synaptic stimulation (100 Hz, 1 s) in the presence of kynurenic acid (2 mM), before and after sequential application of atropine (1 μM) and MPEP (10 μM). Rises in Ca^{2+}, plotted as $\Delta F/F$, were measured in soma and dendrite (15 μm from soma) as indicated on the inset image. *B*, summary data showing the percentage blockade of the Ca^{2+} wave amplitude (mean ± S.E.M.) following bath application of atropine or MPEP, or coapplication of atropine and MPEP. *C*, robust Ca^{2+} waves can be evoked by application of either ACh or (1*S*,3*R*)-1-aminocyclopentane-1,3-dicarboxylic acid (t-ACPD) . Ca^{2+} rises are shown in the same neuron to iontophoretic application of ACh and t-ACPD. *D*, cholinergic and glutamatergic receptor activation act cooperatively to evoke Ca^{2+} waves. The response to somatic iontophoretic application of sub-threshold levels of t-ACPD and ACh is shown along with the response to coapplication of t-ACPD and ACh. *E*, summary data showing that the nuclear Ca^{2+} rise evoked by coapplication of low levels of t-ACPD and ACh is greater than the arithmetic sum of the Ca^{2+} rise evoked by separate applications of ACPD and ACh. *A* and *B*, data were obtained using the Ca^{2+} indicator Oregon Green BAPTA-1 (50 μM). *C*, *D* and *E*, data were obtained using Fluo-5F (300 μM).

dendrite with little reduction in amplitude, and thus did not result from passive diffusion of Ca^{2+} from the initiation point. Agonist-evoked waves also readily invaded the soma and nucleus. There was no obvious difference between the kinetics of waves generated by either mGluR or mAChR stimulation, with either class of agonist being able to evoke a robust Ca^{2+} wave (Fig. 3*C*). As with synaptic stimulation (Fig. 3*A* and *B*), coapplication of the two agonists revealed the cooperative nature of mGluR and mAChR activation on wave generation. Thus, when agonists were applied at levels that evoked little or no Ca^{2+} rise individually, coapplication of the two agonists evoked a large Ca^{2+} wave (Fig. 3*D*). This cooperative action was particularly evident in the large rise in nuclear Ca^{2+} when the two agonists were applied together (Fig. 3*E*). This cooperative activation is most likely to be due to summation of the relatively low levels of IP3 generated by each transmitter on its own and the regenerative nature of Ca^{2+} waves.

Unlike synaptically evoked Ca^{2+} waves that always initiated in the proximal dendrite, the initiation site of agonist-evoked waves was dependent on the location and level of agonist application. Thus, somatic application of agonist resulted in somatic initiation of the wave, which then propagated outward through the dendrite, whereas application of agonist onto the proximal dendrite resulted in dendritic initiation of a wave that propagated toward the soma (Fig. 4*A*). When metabotropic agonists were applied to the proximal dendrites, waves initiated from either the first or second branch point and did not invade higher order dendrites (Fig. 4*B*). In contrast Ca^{2+} rises in response to APs could be seen in all compartments (Fig. 4*B*, right traces). Similar to hippocampal CA1 pyramidal neurons (Nakamura *et al.* 2002), application of agonist onto distal dendrites did not evoke Ca^{2+} rises (mAChR $n = 11$; mGluR $n = 15$). As with synaptically evoked waves, at low stimulus intensities, Ca^{2+} waves were restricted to a local dendritic region with little or no propagation. Increasing the ejection intensity decreased the onset latency, increased the peak amplitude of the Ca^{2+} rises, and increased the distance that the wave propagated ($n = 5$; Fig. 4*C*).

Wave generation requires intracellular Ca^{2+} stores

Ca^{2+} signals evoked by activation of metabotropic receptors in neurons result from generation of IP_3 and subsequent release of Ca^{2+} from IP_3-sensitive intracellular Ca^{2+} stores (Finch & Augustine, 1998; Takechi *et al.* 1998; Nakamura *et al.* 1999; Power & Sah, 2002; Larkum *et al.* 2003). In BLA neurons, waves evoked either synaptically ($n = 3$; Fig. 5*A*) or by exogenous agonist application (t-ACPD, $n = 4$; Ach, $n = 4$; Fig. 5*B*) were completely and reversibly blocked by cyclopiazonic acid (CPA) which blocks the endoplasmic reticulum (ER) Ca^{2+}ATPase and empties intracellular Ca^{2+} stores. We have previously shown (Power & Sah, 2005) that, in BLA neurons, ryanodine receptors (RyRs), are not required for agonist-evoked Ca^{2+} rises, even though they share a common intracellular Ca^{2+} pool with IP_3 receptors. In agreement with this, agonist-evoked waves could not be evoked when the IP_3 receptor antagonist heparin ($500\ \mu g\ ml^{-1}$) was included in the patch pipette ($n = 5$; t-ACPD; data not shown). Synaptically evoked TILL Photonics waves were also blocked by application of 2-aminoethoxydiphenyl borate (2APB; $500\ \mu M$; $n = 3$; Fig. 5*C*), a membrane-permeable blocker of IP_3 receptors and store-operated Ca^{2+} entry (Maruyama *et al.* 1997; Bootman *et al.* 2002*b*; Peppiatt *et al.* 2003) indicating that wave generation requires the production of IP_3 and release of intracellular Ca^{2+} stores. Consistent with this, agonist-evoked Ca^{2+} rises could be mimicked by photolytic uncaging of IP_3, and blocked by emptying stores with CPA (Fig. 5*D*). However, unlike synaptic and agonist-evoked Ca^{2+} rises that had a clear initiation point, photolytic release of IP_3 evoked a near simultaneous Ca^{2+} rise in both the soma and the proximal dendrites, showing that IP_3-sensitive Ca^{2+} stores are present in both locations. Ca^{2+} rises were generally not associated with any change in membrane potential or whole-cell current, consistent with Ca^{2+} release from intracellular Ca^{2+} stores. However occasionally, Ca^{2+} rises were accompanied by a membrane hyperpolarization (Fig. 5*B* and *D*, lower traces) or an outward current in voltage clamp. Both the outward current and the resultant hyperpolarization were also blocked by disruption of IP_3-evoked store release (Fig. 5*B* and *D*), suggesting that the current results from activation of a Ca^{2+}-dependent conductance secondary to release of Ca^{2+} from intracellular stores. This current appears to be mediated by activation of SK Ca^{2+}-activated K^+ channels (Power & Sah, 2006), similar to observations in midbrain dopamine neurons (Fiorillo & Williams, 1998; Morikawa *et al.* 2003) and cortical neurons (Yamada *et al.* 2004; Gulledge & Stuart, 2005).

Metabotropic receptor activation has been also been shown to activate TRP channels in the lateral amygdala (Faber *et al.* 2006) and elsewhere (Ramsey *et al.* 2006). These are mixed cationic channels that have significant Ca^{2+} permeability (Ramsey *et al.* 2006). However, in projection neurons in the basal nucleus, we have not detected any inward current with metabotropic stimulation, despite the large rise in Ca^{2+} in the soma and proximal dendrites. The lack of inward current is also inconsistent with Ca^{2+} influx due to store depletion. Furthermore TRP channel activation and store-operated Ca^{2+} entry are either augmented or unaffected by store depletion (Parekh & Putney, 2005; Ramsey *et al.* 2006). In contrast, depletion of Ca^{2+} stores by application CPA blocks the metabotropic-evoked Ca^{2+} response, while boosting store content by priming augments the metabotropic-evoked Ca^{2+} response (Power & Sah, 2005).

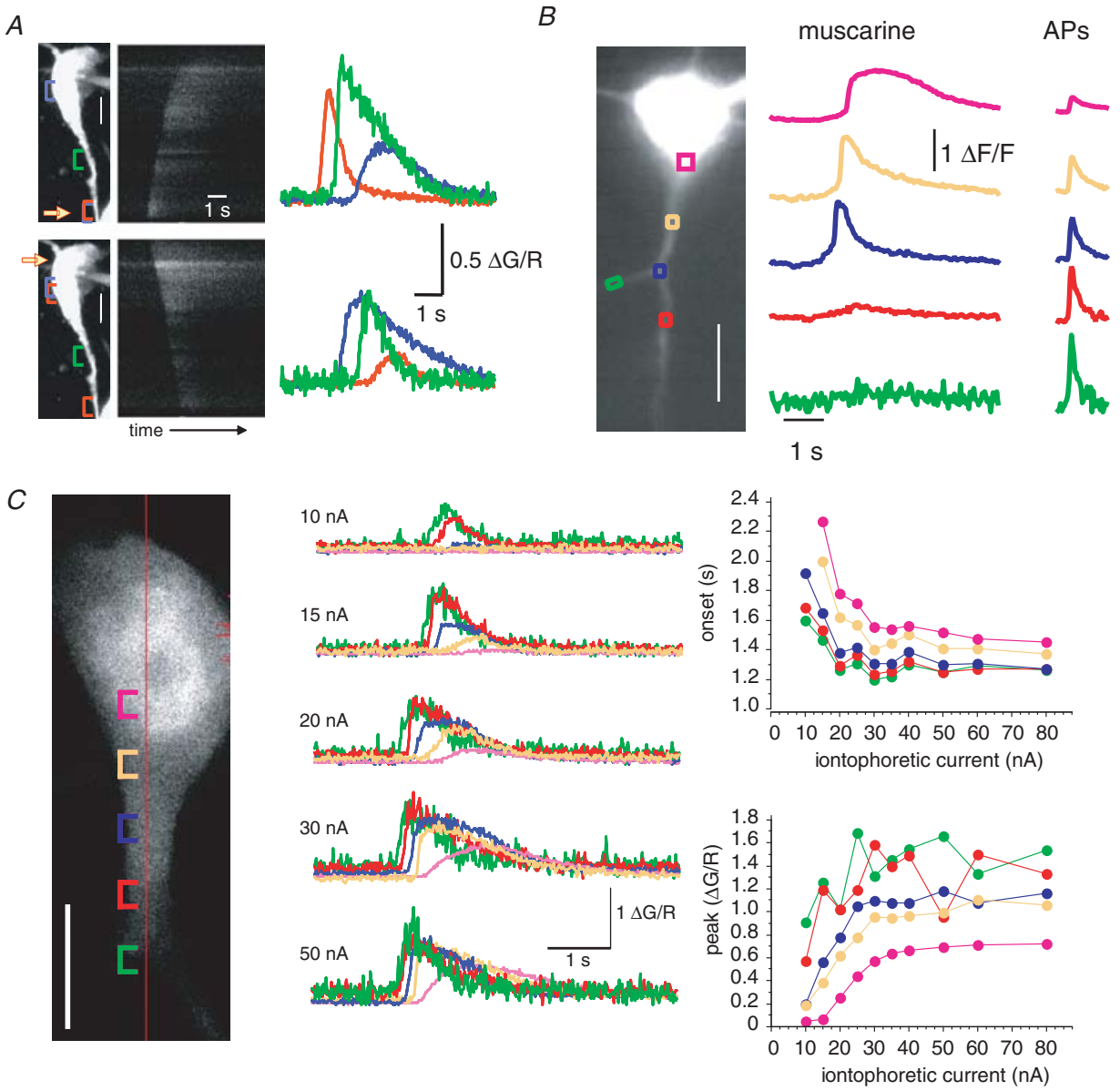

Figure 4. Propagation of agonist-evoked Ca^{2+} waves
A, iontophoretic application of t-ACPD onto the proximal dendrite (top) results in a Ca^{2+} wave that initiates in the dendrite and propagates toward the soma. Application of t-ACPD onto the soma (bottom) produces a wave that propagates from the soma. A projection of the neuron is shown on the left. The yellow arrow indicates the part of the neuron that is closest to the iontophoretic electrode. Scale bar, 5 μm. The middle plot shows the green fluorescence response (indicator, Fluo-5F) for a scan line along the somato-dendritic axis shown on the left over time. Coloured traces in the right panel show rises in Ca^{2+}, plotted as $\Delta G/R$, measured in the soma and along the dendrite as indicated by the coloured brackets in the left panel. *B*, picospritzer application of muscarine (10 μM, 20 p.s.i. (138 kPa), 300 ms) onto the proximal dendrites results in a Ca^{2+} wave that initiates at the first dendritic branch point and propagates toward the soma. The muscarine-evoked Ca^{2+} rise did not propagate along the secondary dendrites (red and green traces). A fluorescence image of the neuron loaded with Oregon Green BAPTA-1 shown on the left together with coloured boxes showing selected regions of interest. Scale bar, 10 μm. Rises in Ca^{2+}, measured along the dendrite as indicated by the coloured boxes are shown in response to muscarine application (middle). The response to a train of four APs (50 Hz) is shown on the right. *C*, increasing agonist stimulation increases wave propagation. The Ca^{2+} rise (coloured traces) evoked by iontophoresis of ACh (50 mM, 1500 ms) onto the proximal dendrite is shown for various intensities of ejection current (indicator, Fluo-5F). Cellular regions of interest along with the scan-line are indicated on the confocal section (left). Graphs of the iontophoretic intensity *versus* onset and peak for each region of interest are shown on the right. Scale bar, 10 μm.

Taken together, our results are consistent with release of Ca^{2+} from IP_3-sensitive intracellular Ca^{2+} stores being necessary for Ca^{2+} wave generation in BLA projection neurons.

Distribution of Ca^{2+} release in BLA projection neurons

In hippocampal and cortical pyramidal neurons, metabotropic-receptor evoked Ca^{2+} rises are largely restricted to the soma and proximal apical dendrite (Nakamura *et al.* 2000; Larkum *et al.* 2003). Although the amygdala is not a layered structure, projection neurons in the BLA are often described as 'pyramidal-like' (McDonald, 1992; Washburn & Moises, 1992*a*; Sah *et al.* 2003). Indeed, some projection neurons in the basal nucleus have a stereotypical pyramidal morphology, with a single long, broad ($>1.5\,\mu$m diameter) 'apical-like' dendrite emanating from the soma, and a number of thin ($<1.5\,\mu$m diameter) rapidly branching 'basal-like' dendrites radiating from the soma. However, similar to previous observations (McDonald, 1982; Rainnie & Shinnick-Gallagher, 1992; Washburn & Moises, 1992*a*), projection neurons were often found to be multipolar, with multiple broad dendrites radiating from the soma (e.g. Fig. 7*A*). Morphological examination of dye-filled BLA projection neurons revealed that, as in many other

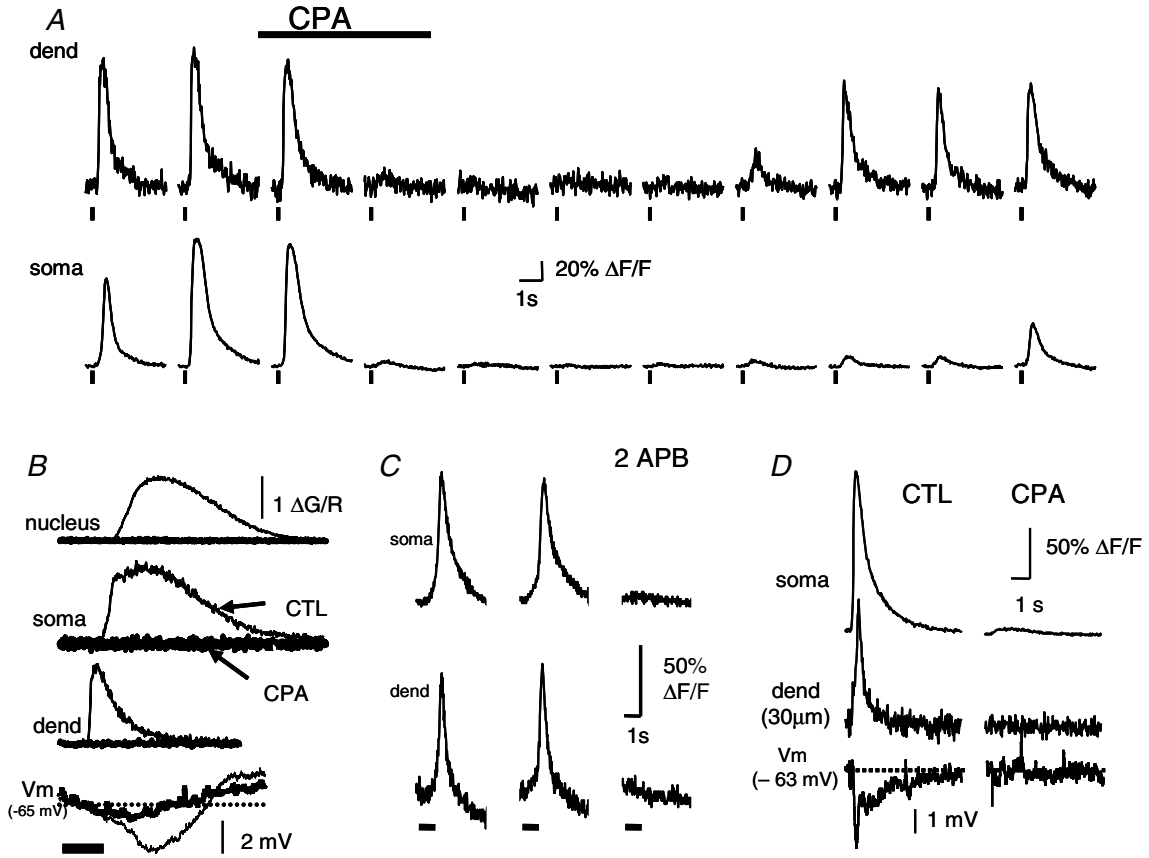

Figure 5. Ca^{2+} waves require release of Ca^{2+} from inositol 1,4,5-trisphosphate (IP_3)-sensitive intracellular Ca^{2+} stores

A, cyclopiazonic acid (CPA, 30 μM) reversibly blocks synaptically evoked Ca^{2+} waves. Waves were evoked by external capsule stimulation (100 Hz, 250 ms) at 5 min intervals under voltage clamp (HP −70 mV; indicator, Oregon Green BAPTA-1). Neurons were depolarized to −50 mV between tetani to maintain Ca^{2+} stores. Changes in dendritic and somatic Ca^{2+} ($\Delta F/F$) are plotted before application of CPA, in the presence of CPA (5 min and 10 min), and during washout of CPA. *B*, CPA blocks agonist-evoked Ca^{2+} waves. Ca^{2+} rises, plotted as $\Delta G/R$ (indicator, 300 μM Fluo-5F), and the voltage response evoked by iontophoretic application of t-ACPD (bottom traces) are shown before (thin traces) and 15 min after (bold traces) application of CPA (30 μM). *C*, rises in Oregon Green BAPTA-1 fluorescence evoked by external capsule stimulation (100 Hz, 1 s) before (left and middle) and 5–10 min after application of 2-aminoethoxydiphenyl borate (2APB; 500 μM; right). The bar beneath the fluorescence traces indicates the timing of synaptic stimulation. *D*, Ca^{2+} rises evoked by the photolytic uncaging of IP_3 (50 μM caged IP_3 and 50 μM Oregon Green BAPTA-1 in pipette), and the voltage change in response to the Ca^{2+} change (bottom traces), are blocked by bath application of CPA (10 min, 30 μM).

pyramidal neurons (Elston & DeFelipe, 2002), the primary branch of the 'apical-like' dendrites contains few if any spines. Secondary branches are thinner and generally spiny while tertiary and higher branch orders are thin and spine dense (>0.5 spines μm^{-1}). The spine density of the primary and secondary branches of 'basal-like' dendrites is heterogeneous, ranging from few if any spines to spine dense. Tertiary and higher order branches of these basal processes are spine dense. As shown above, the soma and proximal dendrite of BLA projection neurons contain intracellular Ca^{2+} stores that can be released by generation of IP_3. We next determined the distribution of these Ca^{2+} stores through the dendritic tree.

As shown in Fig. 4*B*, metabotropic-evoked Ca^{2+} rises were only observed in the soma and proximal dendrites. The absence of metabotropic receptor-evoked Ca^{2+} rises in the distal dendrites could reflect a differential distribution of metabotropic receptors, IP_3 receptors or intracellular Ca^{2+} stores. However, because of the Ca^{2+} dependence of the IP_3 receptor (Iino, 1990; Bezprozvanny *et al.* 1991; Finch *et al.* 1991; Mak *et al.* 1998), it is conceivable that differences in resting Ca^{2+} between proximal and distal compartments could also contribute to their ability to evoke Ca^{2+} waves. As Ca^{2+} and IP_3 act as coagonists at IP_3 receptors (Bezprozvanny *et al.* 1991; Finch *et al.* 1991; Mak *et al.* 1998), rises in free Ca^{2+} from Ca^{2+} influx during APs in the presence of IP_3 can amplify Ca^{2+} transients by IP_3-CICR (Taylor & Marshall, 1992; Nakamura *et al.* 1999). When the level of applied agonist was reduced to levels that failed to evoke a Ca^{2+} wave, pairing agonist application with APs resulted in an augmented Ca^{2+} response ($n = 5$; Fig. 6). Thus, IP_3-CICR provides a robust method to assess the presence of intracellular Ca^{2+} stores that express IP_3 receptors.

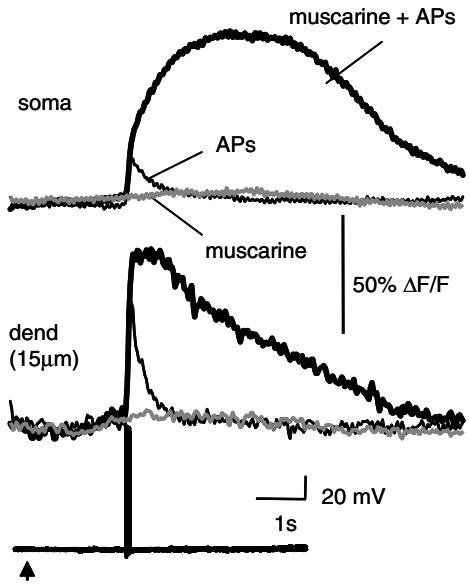

Figure 6. Amplification of AP-evoked Ca^{2+} rises by metabotropic receptor stimulation
Ca^{2+} rises in the soma and proximal dendrite (indicator, Oregon Green BAPTA-1) are shown in response to picospritzer application of muscarine (10 μM; grey traces), a train of four APs (50 Hz; thin traces), and an AP train delivered immediately following application of muscarine (bold traces). The voltage responses are shown below the Ca^{2+} responses. The arrow indicates the timing of the muscarine application (100 ms, 20 p.s.i. (138 kPa)).

To assess the metabotropic receptor-mediated Ca^{2+}-response potential of dendritic segments, neurons were loaded with the moderate affinity indicator Fluo-5F and imaged using two-photon microscopy. IP_3-CICR was assayed over different neuronal compartments by comparing the Ca^{2+} rise evoked by AP trains with and without coapplication of t-ACPD or muscarine. To maximize our ability to detect store release, we applied agonists at concentrations that evoked robust waves in the soma and evoked APs using a two spike-train protocol (two 100 Hz trains of four APs were given with a 200 ms intertrain interval). Under control conditions, as in pyramidal neurons (Markram *et al.* 1995; Sah & Clements, 1999), the AP-evoked Ca^{2+} rise was greatest in the thin spine-dense dendritic segments, slightly smaller in the broad spine-sparse proximal dendrites, much smaller in the soma and almost negligible in the nucleus (Fig. 7*B* and *C*). Local application of t-ACPD produced a marked augmentation of the AP-evoked Ca^{2+} response in the nucleus, soma, and proximal dendrites (Fig. 7, Table 1). In the presence of t-ACPD, both the peak and the integrated area of the AP-evoked Ca^{2+} rise were dramatically larger in the soma, nucleus and primary dendrites.

In secondary branches, while amplification was clearly present, it was significantly lower than that observed in primary dendrites (amplitude $P < 0.001$; area $P < 0.01$). In contrast, no significant amplification of the Ca^{2+} transient was detected in higher-order branches. Close examination of the dendritic tree (see Methods) also revealed a wide variation in spine density (0.1–2.2 spines μm^{-1}). We found that the level of Ca^{2+} amplification was correlated with the spine density (Fig. 7*D*). Thus, amplification was significantly greater in spine-sparse branches (<0.5 spines μm^{-1}) than in spine-dense branches (>0.5 spines μm^{-1}). The amplification of Ca^{2+} rises in all compartments was due to release from intracellular Ca^{2+} stores as, in the presence of CPA, t-ACPD had no effect on either the amplitude or the integrated area of the AP-evoked Ca^{2+} rise (Fig. 7*E* and *F*, Table 2) and no amplification was observed when the IP_3 antagonist heparin was included in the patch pipette (Fig. 7*G*, Table 2).

Application of cholinergic agonists also augmented the AP-evoked Ca^{2+} rise. The distribution of cholinergic-mediated IP_3-CICR was strikingly similar to the IP_3-CICR evoked by mGluR stimulation (Fig. 8).

Cholinergic-evoked store release was restricted to the nucleus, soma and proximal dendrites. mAChR agonists increased the peak of the AP-evoked Ca^{2+} rise (Fig. 8*Ba*) by $200 \pm 39\%$ in the soma ($P < 0.0001$; $n = 13$), $441 \pm 83\%$ in the nucleus ($P < 0.0001$; $n = 10$), $56 \pm 16\%$ in primary branches ($P < 0.01$; $n = 15$), and $39 \pm 20\%$ in secondary branches ($P < 0.05$; $n = 12$). mAChR agonists increased the integrated area (Fig. 8*Bb*) of the AP-evoked Ca^{2+} rise in by $930 \pm 198\%$ in the soma ($P < 0.001$; $n = 13$), $927 \pm 175\%$ in the nucleus ($P < 0.01$; $n = 10$), $319 \pm 87\%$ in primary branches ($P < 0.01$; $n = 15$), and $166 \pm 62\%$ in secondary branches ($P < 0.05$; $n = 12$). No significant amplification of either the peak ($P = 0.90$) or the integrated area ($P = 0.19$) was observed in higher order branches ($n = 11$). Similar to the effects seen with t-ACPD, mAChR-mediated store release tended to be more pronounced in spine-sparse branches. Cholinergic effects were the result of mAChR activation, as they could be evoked by application of ACh or muscarine and were fully blocked by atropine ($n = 5$). Cholinergic IP_3-CICR was fully blocked by CPA ($n = 5$; Fig. 8*D* and *E*). Finally, IP_3-CICR was also observed, albeit to a lesser degree, in response to bath application of muscarine (Fig. 8*F*). IP_3-CICR evoked by bath application of agonist was also restricted to the soma and spine-sparse dendrites. The similar distribution of IP_3-CICR evoked by focal and bath-application of agonist suggests that the lack of IP_3-CICR in higher-order dendrites to focal application agonists was not because focal application of agonist does not generate sufficient levels of IP_3.

We next compared the distribution of synaptically activated IP_3-CICR with the distribution of IP_3-CICR obtained with exogenous application of agonist. Similar to results obtained with low levels of metabotropic agonists (Fig. 6), tetanic synaptic stimulation below the threshold for evoking a Ca^{2+} wave was found to augment the AP-evoked Ca^{2+} response. This augmented Ca^{2+} response was also only observed in the soma and proximal dendrites (Fig. 9*A*). As expected from activation of metabotropic receptors, tetanic synaptic stimulation also blocked the slow afterhyperpolarization that followed trains of APs (Womble & Moises, 1993, 1994; Faber & Sah, 2002). We also examined whether pairing APs with synaptic stimulation augments nuclear Ca^{2+}. To test this possibility, we first applied local tetanic stimuli at levels to evoke a small Ca^{2+} rise that was restricted to the proximal dendrite (Fig. 9*B* and *C*), similar to that obtained with low levels of exogenous agonist application (Fig. 4*C*). As shown previously (Fig. 7), AP trains led to a robust Ca^{2+} rise in distal dendrites but only small Ca^{2+} rises in the nucleus. Pairing synaptic simulation with AP trains resulted in a large rise in nuclear Ca^{2+} that lasted several seconds (Fig. 9*C*). The integrated area of fluorescence response in the nucleus to paired synaptic stimulation and AP trains was 2.37 ± 0.52 times greater than the arithmetic sum the sum of the unpaired presentations of synaptic and AP stimuli ($n = 4$; $P < 0.05$; Fig. 9*D* and *E*).

Why does IP_3-CICR show such a restricted distribution? The distribution of intracellular Ca^{2+} stores (endoplasmic reticulum) is not known in BLA projection neurons, so the lack of store release may be due to the absence of stores in spine-dense regions of the dendritic tree. Alternatively, it may reflect a differential distribution of either metabotropic receptors, IP_3 receptors, or, as in cultured neurons, some of the subcellular components of the IP_3 signalling pathway (Jacob *et al.* 2005). To test whether the distribution of IP_3-sensitive Ca^{2+} stores underlies the restricted distribution of metabotropic-evoked store release we loaded neurons with 50–100 μM of caged IP_3 and Oregon Green BAPTA-1 (50 μM) for 15–20 min. To ensure adequate UV light penetration, we restricted our examination to dendrites that were near the surface of the slice (at the same level or closer to the surface than the soma). Under these conditions, AP trains evoked Ca^{2+} rises throughout the neuron. However, Ca^{2+} rises evoked by photolysis of caged IP_3 were restricted to the soma and proximal dendrites (Fig. 10*A* and *B*). No detectable rise in Ca^{2+} was seen in the distal dendrites two or more branch points removed from the soma. Furthermore, pairing the photo-release of IP_3 with AP trains (four APs, 50 Hz) produced no significant augmentation of the AP-evoked Ca^{2+} in the distal dendrites (Fig. 10*C* and *D*). The amplitude of the paired response in the distal dendrites was $101 \pm 9\%$ of the AP only response ($P = 0.33$; $n = 9$). As with agonist application, the area of the paired response in the distal dendrites tended to be enhanced ($125 \pm 12\%$; $P = 0.11$; $n = 9$), but this difference was not significant. The lack of an IP_3-mediated Ca^{2+} response in the distal dendrites is unlikely to be due to an inability to uncage IP_3, since the response to the photolytic uncaging of Ca^{2+} was similar in the soma and distal dendrites (data not shown). These results suggest that the proximal distribution of metabotropic-mediated store release is most likely to result from a differential distribution of IP_3 receptors.

Discussion

In this study we have characterized Ca^{2+} release from intracellular stores in projection neurons in the BLA. We show that synaptic activation of mGluRs or mAChRs leads to a focal rise in cytosolic free Ca^{2+} in the dendrite that propagates as a wave to the soma and invades the nucleus. This wave results from generation of IP_3 and Ca^{2+} release from IP_3-sensitive Ca^{2+} stores. Pairing of APs with synaptic stimulation leads to amplification of Ca^{2+} transients by IP_3-receptor-dependent CICR in both the soma and the proximal dendrite, with the largest rise occurring in the nucleus. These triggered rises in nuclear Ca^{2+} may underlie the cellular changes that accompany BLA-dependent learning.

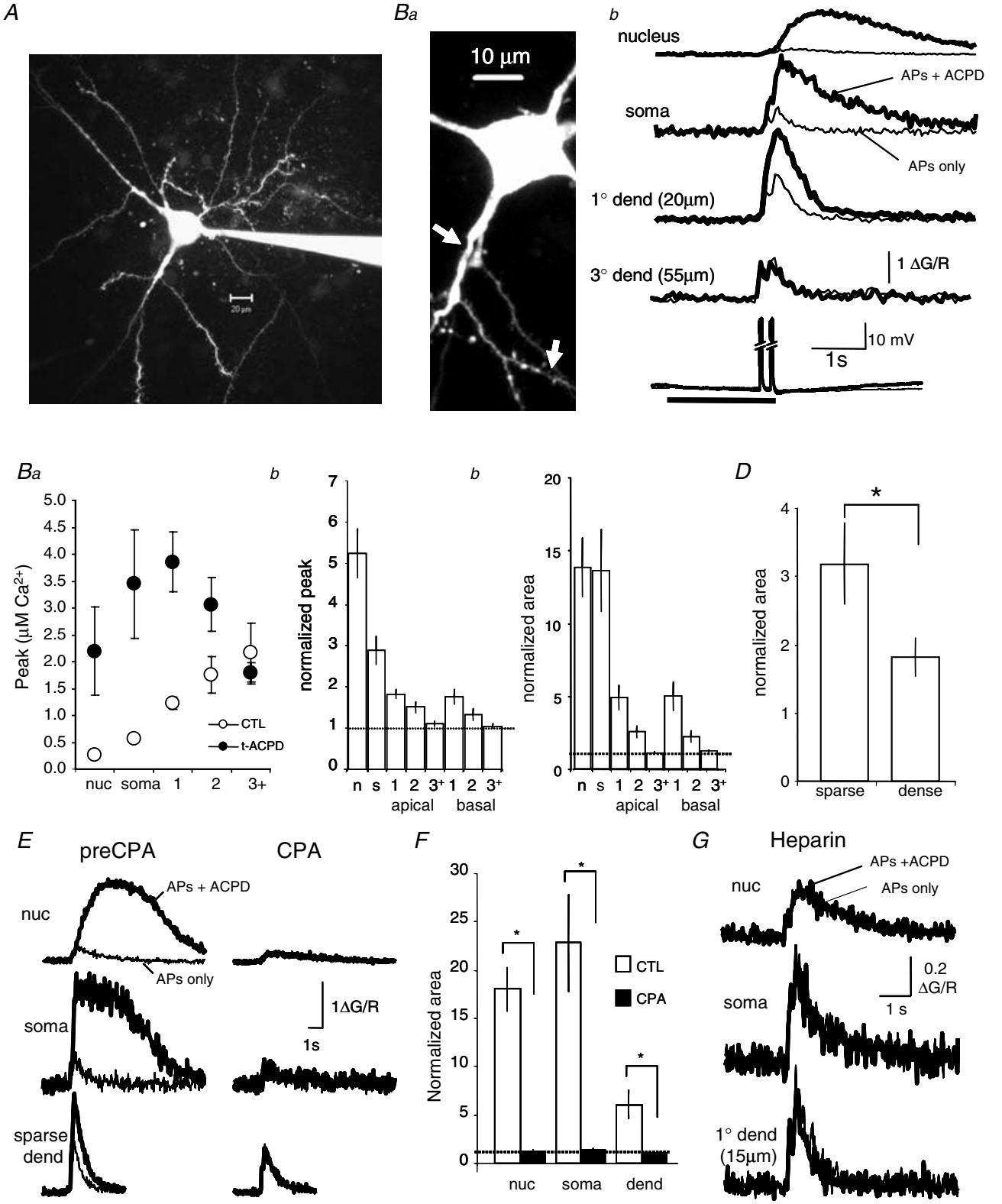

Figure 7. mGluR-mediated amplification of AP-evoked Ca^{2+} rises are localized to the soma and proximal dendrites

A, two-dimensional projection of a confocal image stack (Alexa 594). Note that two broad 'apical-like' dendrites can be seen projecting from the soma. *B*, amplification of AP-evoked rises by t-ACPD is differentially distributed throughout the dendritic tree. Application of t-ACPD to the soma or primary 'apical-like' dendrite augments the

Table 1. Distribution of t-ACPD-mediated IP_3-CICR

	n	Amplitude	*P*	Area	*P*
Nucleus	10	5.24 ± 0.59	<0.001	13.68 ± 1.98	<0.01
Soma	13	2.89 ± 0.35	<0.001	13.48 ± 2.79	<0.01
1° apical	20	1.82 ± 0.11	<0.0001	4.83 ± 0.83	<0.01
2° apical	19	1.51 ± 0.13	<0.001	2.51 ± 0.41	<0.01
3+ apical	6	1.11 ± 0.07	0.21	1.08 ± 0.07	0.24
1° basal	15	1.76 ± 0.19	<0.001	4.93 ± 0.99	<0.01
2° basal	13	1.34 ± 0.14	<0.05	2.18 ± 0.41	<0.05
3+ basal	9	1.05 ± 0.05	0.52	1.19 ± 0.08	0.19

t-ACPD, (1*S*,3*R*)-1-aminocyclopentane-1,3-dicarboxylic acid; IP_3-CICR, Ca^{2+}-induced Ca^{2+} release at IP_3 receptors; *n*, number of neurons. The amplitude and integrated area of the Ca^{2+} transient in the presence of t-ACPD were normalized to the AP-only values (mean ± S.E.M.) for each region of interest. *P* values were calculated using a paired *t* test.

Table 2. mGluR augmentation of the AP-evoked Ca^{2+} rise requires IP_3 receptor activation

	CTL	Heparin	Pre-CPA	CPA
Amplitude				
Nucleus	5.24 ± 0.59 (10)	1.08 ± 0.16 (4)*	6.50 ± 0.50 (4)	1.11 ± 0.17 (4)**
Soma	2.89 ± 0.35 (13)	0.94 ± 0.01 (4)*	3.87 ± 0.39 (4)	0.90 ± 0.07 (4)**
1° apical	1.82 ± 0.11 (20)	1.17 ± 0.28 (4)*	2.09 ± 0.27 (5)	0.88 ± 0.08 (5)**
Area				
Nucleus	13.68 ± 1.98 (10)	0.85 ± 0.16 (4)*	18.02 ± 2.23 (4)	1.24 ± 0.15 (4)**
Soma	13.48 ± 2.79 (13)	1.07 ± 0.20 (4)*	22.82 ± 4.98 (4)	1.35 ± 0.23 (4)*
1° apical	4.83 ± 0.83 (20)	1.24 ± 0.30 (3)*	6.10 ± 1.42 (5)	1.03 ± 0.08 (5)*

The amplitude and integrated area of the AP Ca^{2+} transient in the presence of t-ACPD, normalized to AP Ca^{2+} transient in the absence of t-ACPD, are given for each region of interest under drug-free control conditions (CTL), when heparin was included in the patch pipette, and before and during bath application of cyclopiazonic acid (CPA). The number of neurons is given in parentheses. $^*P < 0.05$, $^{**}P < 0.01$.

Neurons in the BLA receive glutamatergic as well as dense cholinergic innervation (Ben-Ari *et al.* 1977). We have found that these two transmitter systems act cooperatively to release intracellular Ca^{2+} (Fig. 3). Synaptic stimulation of local afferents to BLA neurons activates both types of afferents. Thus, Ca^{2+} waves are attenuated by >70% when muscarinic receptors are blocked by atropine, and by 40–65% when mGluR5 receptors are blocked by MPEP (Fig. 3). This cooperative action is most likely to be due to summation of the

AP-evoked Ca^{2+} rise in the nucleus, soma, and primary 'apical-like' dendrite. Application of t-ACPD onto the tertiary dendrite (3° dend) has little or no effect on the AP Ca^{2+} response in the tertiary dendrite. The Ca^{2+} rise evoked by two AP trains (four APs at 100 Hz) is shown with (bold traces) and without (thin traces) iontophoretic application of t-ACPD. Regions where measurements were made on the primary and tertiary dendrites are indicated by the arrows in *a*. *Ca*, summary data showing the amplitude of the AP-evoked Ca^{2+} rise with and without application of t-ACPD to the nucleus (nuc), soma (soma), primary (1), secondary (2) and higher-order (3+) dendritic branches. *Cb* and *c,* summary data illustrating the peak amplitude (*b*) and area (*c*) of the AP-evoked Ca^{2+} rise in the presence of t-ACPD normalized to the AP-only response. *D,* the mGluR-mediated augmentation of the AP-evoked Ca^{2+} rise was greater in spine-sparse ($n = 11$) than in spine-dense ($n = 18$) dendritic segments (unpaired *t* test $P < 0.05$). Bars show the integrated area of the AP-evoked Ca^{2+} response in the presence of t-ACPD, normalized to the AP-only response, for secondary dendritic branches which are spine sparse (<0.5 spines μm^{-1}) and spine-dense (>0.5 spines μm^{-1}). *E*, augmentation of AP-evoked Ca^{2+} response in the presence of t-ACPD (bold traces) is blocked by CPA (thin traces). *F*, summary data showing the integrated area of the AP-evoked Ca^{2+} rise in the presence of t-ACPD, normalized to the AP-evoked response in the absence of t-ACPD, before and after bath application of CPA (30 μM). *G*, when heparin was included in the patch pipette, coapplication of t-ACPD (bold traces) had no effect on the AP-evoked Ca^{2+} response (thin traces). Bars indicate means ± S.E.M. $^*P < 0.05$.

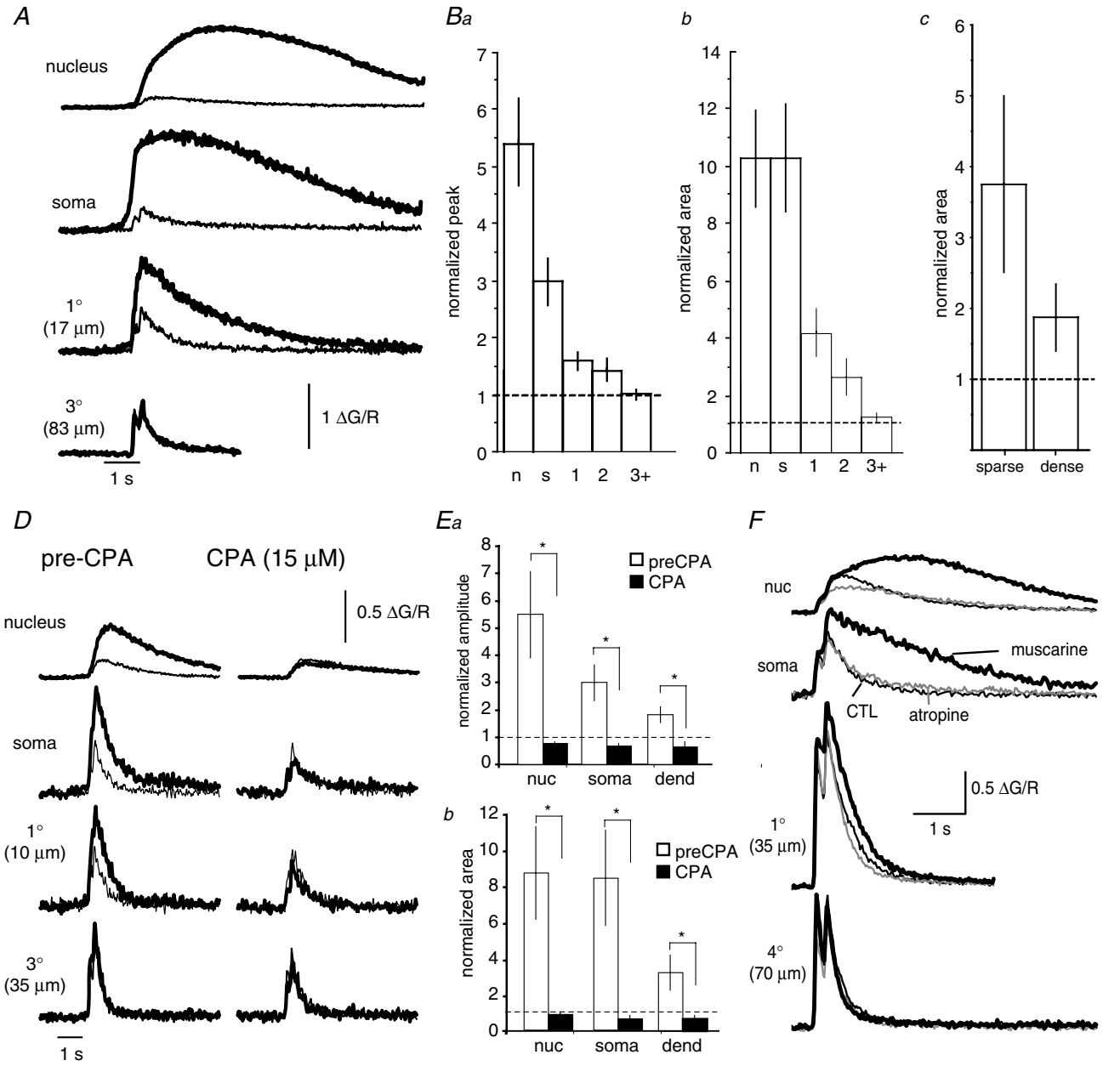

Figure 8. Distribution of AChR-mediated Ca^{2+} rises
A, amplification of AP-evoked Ca^{2+} rises evoked by mAChR activation is differentially distributed throughout the dendritic tree. The Ca^{2+} rise evoked by AP trains is shown with (bold traces) and without (thin traces) iontophoretic application of ACh (20 mM, 1 s) to various cellular regions (indicator, Fluo-5F). *B*, summary data showing the amplification of the peak amplitude (*a*) and integrated area (*b*) of the AP-evoked Ca^{2+} rise with and without mAChR stimulation in the nucleus (n), soma (s), primary (1), secondary (2) and higher order (3+) dendritic branches. *C*, bars show the mAChR-evoked amplification of the AP-evoked Ca^{2+} transient for secondary branches that are classified as either spine-sparse ($n = 5$) or spine-dense ($n = 7$). *D*, augmentation of the AP-evoked Ca^{2+} response by ACh (bold traces) is blocked by CPA (15 μM). *E*, summary data showing ACh-mediated amplification of the amplitude (*a*) and integrated area (*b*) of the AP-evoked Ca^{2+} rise before and after bath-application of CPA (30 μM; $n = 5$). $^*P < 0.05$. *F*, bath-application of muscarine (5 μM) augments the AP-evoked Ca^{2+} response in the soma and proximal dendrites, but is without effect on more distal dendrites. The AP-evoked Ca^{2+} rise, plotted as $\Delta G/R$ (indicator, Fluo-5F), is shown before (thin traces) and after bath-application of muscarine (bold traces) measured at the indicated cellular compartments. Muscarinic augmentation of the AP Ca^{2+} signal was blocked by atropine (1 μM; grey traces). *B*, *C* and *E*, the AP-evoked Ca^{2+} response in the presence of ACh is normalized to the AP-evoked Ca^{2+} response in the absence of ACh for each region of interest.

relatively low levels of IP_3 generated by each transmitter on its own. As Ca^{2+} release from IP_3-sensitive stores is a regenerative function, coapplication evokes a superlinear Ca^{2+} response (Fig. 3*C* and *D*).

In BLA neurons, IP_3-evoked Ca^{2+} responses are most prominent in the soma and primary dendrites. For the dendritic tree, there is an inverse correlation between spine density and the capacity of metabotropic receptor activity to evoke IP_3-mediated Ca^{2+} release in secondary dendrites. Thus, store release is present in dendrites that have a low density of spines (primary and secondary dendrites) but is greatly reduced or absent in spine-dense regions. A similar distribution has been suggested in hippocampal and cortical pyramidal cells where regenerative release of Ca^{2+} from IP_3-sensitive stores in response to metabotropic receptor activation has been found almost exclusively in the soma and spine-sparse proximal apical dendritic shaft (Kapur *et al.* 2001; Nakamura *et al.* 2002; Power & Sah, 2002; Larkum *et al.* 2003), but not in the spine-dense oblique branches

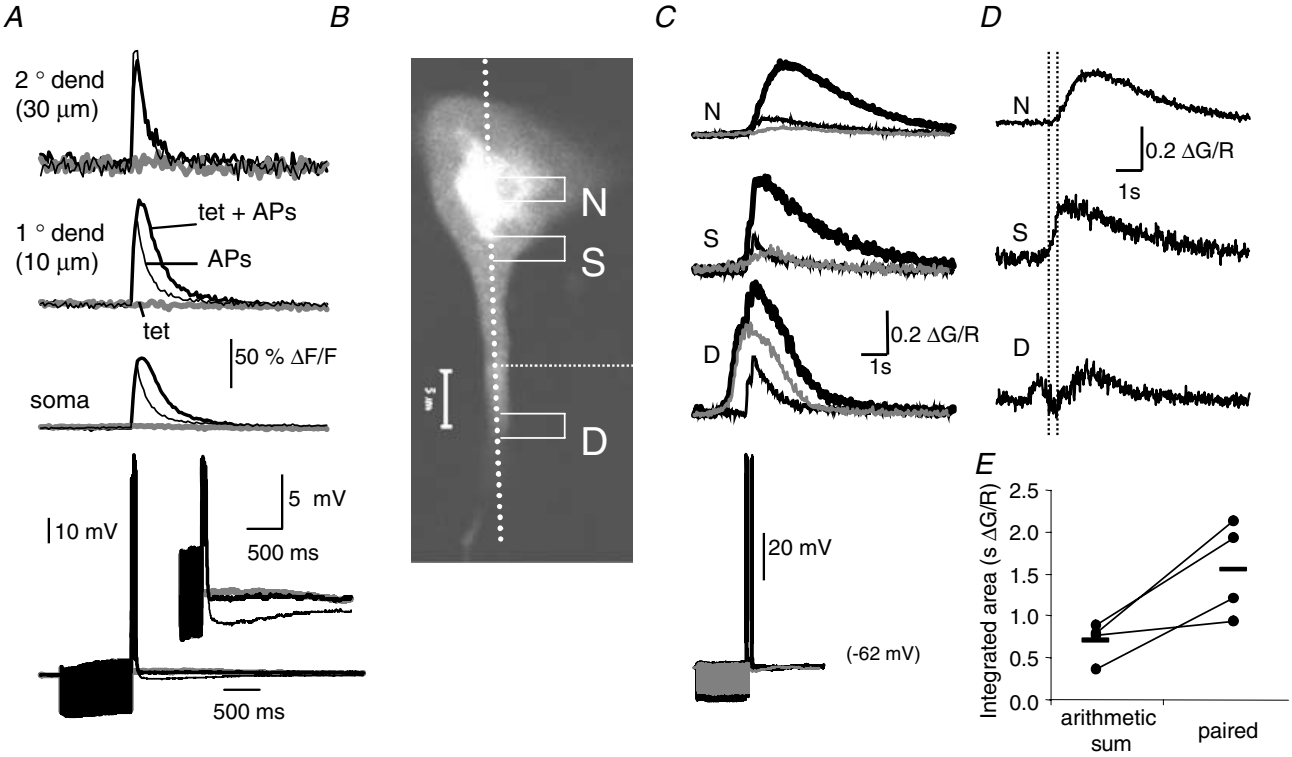

Figure 9. Synaptic stimulation leads to Ca^{2+}-induced Ca^{2+} release at IP_3 receptors (IP_3-CICR) in the nucleus

A, Ca^{2+} rises in the soma and dendrite (indicator, Oregon Green BAPTA-1) are shown in response to local synaptic stimulation (100 Hz, 1 s; grey traces), in the presence of 2-amino-5-phosphonovaleric acid (APV; 60 μM) and 6-cyano-7-nitroquinoxaline-2,3-dione (CNQX; 20 μM), to a train of four APs (50 Hz; thin black traces), and to an AP train delivered during synaptic stimulation (bold black traces). Voltage responses are plotted below the fluorescence responses. The inset voltage traces show an expanded view of the slow afterhyperpolarization that follows the AP train. Note the suppression of the slow afterhyperpolarization following tetanic stimulation. *B*, confocal red fluorescence image of a BLA projection neuron loaded with Fluo-5F (300 μM) and Alexa 594 (30 μM) showing the location of the scan line along with the nuclear (N) and somatic (S) and dendritic (D) regions of interest. *C*, pairing local synaptic stimulation (50 Hz, 2 s) with two AP trains (four APs 100 Hz, 200 ms intertrain interval) evoked a nuclear Ca^{2+} response that was greater than the sum of the AP and synaptically evoked responses. The Ca^{2+} rise evoked by AP trains (thin traces), synaptic stimulation (grey traces), and AP trains paired with synaptic stimulation (bold traces) are shown for the regions of interest indicated in *B*. Voltage responses are shown below the fluorescence responses. APV (30 μM) and NBQX (10 μM) were present in the bath. Note that the wave evoked by unpaired synaptic stimulation failed to invade the nucleus. The responses to paired stimulation showing the component due to amplified Ca^{2+} release obtained by subtracting the AP and synaptic responses are shown in *D*. Note the supra-linear response in each compartment. Dashed lines indicate the timing of the AP trains. *E*, the nuclear Ca^{2+} response to paired presentations of APs and synaptic stimulation (50 Hz, 1–2 s) was greater than the arithmetic sum of the responses to unpaired presentations. The line plot shows the integrated area of the nuclear Ca^{2+} responses to paired synaptic and AP stimulation, along with the arithmetic sum of unpaired presentations for individual neurons. Individual values are an average of 2–4 repetitions. Dashes indicate the group mean ($n = 4$).

(Nakamura *et al.* 2002). Why does IP_3-CICR show such a restricted distribution? The possibilities are that it may reflect a differential distribution of either metabotropic receptors, IP_3 receptors or, as in cultured neurons, some of the subcellular components of the IP_3 signalling pathway (Jacob *et al.* 2005). In hippocampus (Marino *et al.* 1998) and cortex (Mrzljak *et al.* 1993), M1 mAChRs, which are coupled to phosphoinositide hydrolysis (Caulfield, 1993), are found on the soma, proximal and distal dendrites, as well as on the spine head. Group I mGluR receptors

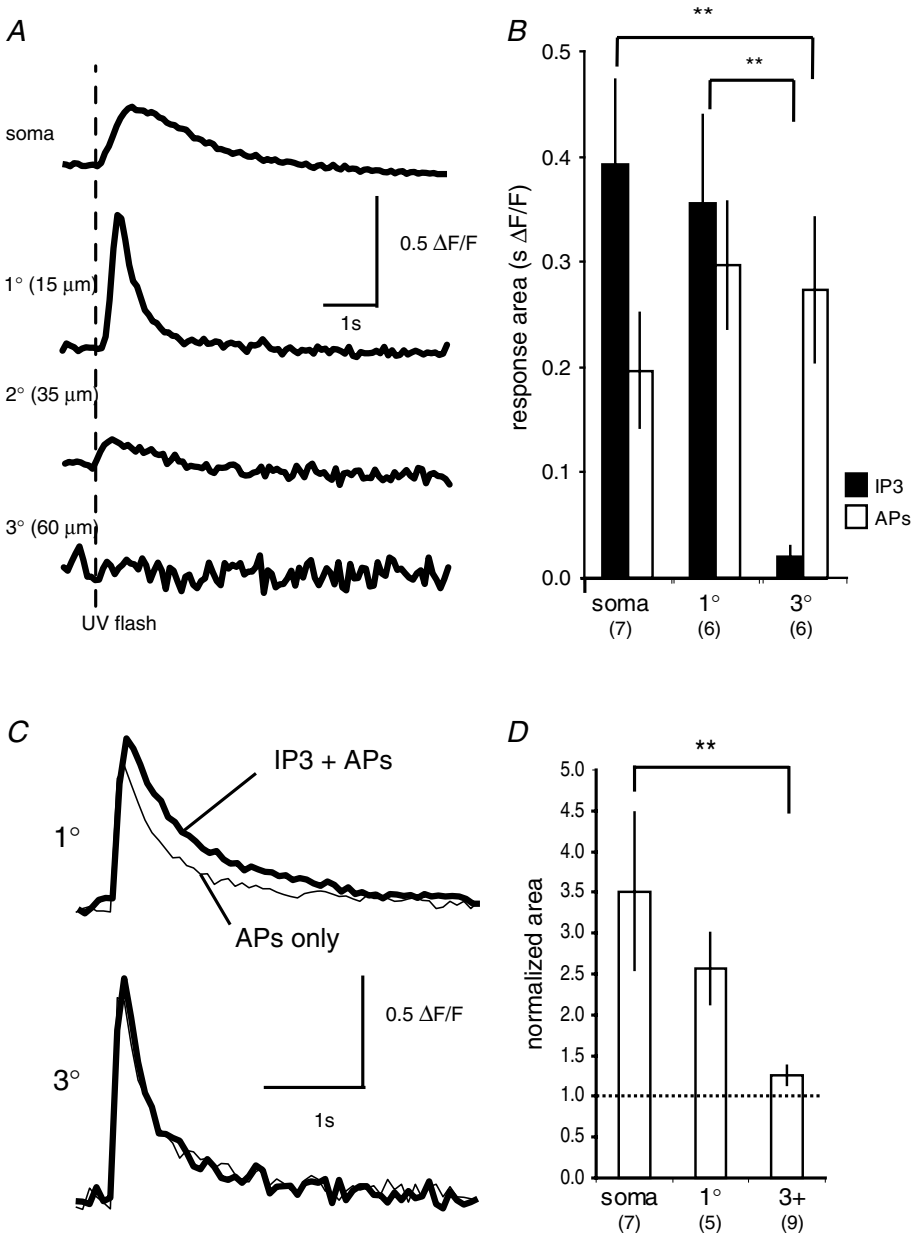

Figure 10. Ca^{2+} rise evoked by IP_3 uncaging is restricted to the soma and proximal dendrites
A, the Ca^{2+} response, plotted as $\Delta F/F$ (Oregon Green BAPTA-1, 50 μM), to photolytic uncaging of IP_3 (75 μM) is shown for the soma, and segments of the primary, secondary and tertiary dendrites. The dashed line indicates the timing of the UV flash. *B*, summary data showing the integrated area (mean ± S.E.M.) of the Ca^{2+} rise evoked by uncaging of IP_3 and AP trains for the soma, primary dendrite (1°), and tertiary dendrite (3°). The number of neurons in each group is indicated in parentheses. $^{**}P < 0.01$ (Fisher's PLSD *post hoc* test). *C*, the AP-evoked Ca^{2+} response in the distal dendrites is unaffected by photolytic uncaging of IP_3. The Ca^{2+} rise evoked by an AP train (four APs at 50 Hz) is shown with (bold traces) and without (thin traces) photolytic uncaging of IP_3, in the primary (1°) and tertiary (3°) dendrites. *D*, summary data illustrating the area of the AP-evoked Ca^{2+} rise when APs were paired with photolytic uncaging of IP_3, normalized to the responses to the APs alone for the soma, primary (1°) and tertiary (3°) dendrites. The number of neurons in each group is indicated in parentheses. $^{**}P < 0.01$ (Fisher's PLSD *post hoc* test).

are localized on the soma and dendrites, and they are particularly prevalent the spines (Lujan *et al.* 1997). In the basal nucleus, cholinergic terminals have been shown to make contact with soma, dendrites and spines (Carlsen & Heimer, 1986; Li *et al.* 2001); however, the subcellular distribution of mAChR subtypes in is unknown. While the distribution of mGluR subtypes in the basal nucleus is not known, mGluR-5 receptors in the lateral amygdala are located primarily on spines and dendrites, and to a lesser extent on the soma (Rodrigues *et al.* 2002). Our data show that the Ca^{2+} response to IP_3 photolysis is also restricted to the soma and proximal dendrites. Thus, the restricted distribution of Ca^{2+} waves and IP_3-CICR reflects in part differences in the distribution of IP_3 receptors: either a difference in IP_3 receptor density, or a difference in the sensitivity of the receptor to IP_3 such that IP_3 receptors located proximally are more readily activated.

As in other neuronal types (Nakamura *et al.* 1999; Kapur *et al.* 2001; Power & Sah, 2002; Larkum *et al.* 2003), Ca^{2+} waves evoked by synaptic stimulation in BLA neurons always initiated in the dendrite (the first or second branch point) and propagated toward the soma. Wave generation has been modelled in neurons by Ross and colleagues (Nakamura *et al.* 2002). In their model, IP_3 is generated by activation of metabotropic receptors located on spine-dense dendrites and diffuses to IP_3 receptors preferentially localized on the proximal dendrites (Nakamura *et al.* 2002). Our data are consistent with this model in that (1) not only is the Ca^{2+} response to IP_3 photolysis restricted to the soma and proximal dendrite, but it rises simultaneously in the soma and proximal dendrite (Fig. 5*C*), (2) agonist evoked waves were found to propagate away from the source of stimulation. Thus, waves evoked by somatic application of agonist propagated from the soma outward through the dendrite, whereas waves evoked by dendritic application of agonist propagated from the dendrite toward the soma (Fig. 4*A*). As synaptically generated waves always propagate from the dendrite to the soma, it is likely that much of the IP_3 is generated in the dendrites. In the BLA, synaptically evoked Ca^{2+} waves readily invaded the soma and nucleus. In CA1 pyramidal neurons, it has been reported that synaptically evoked waves rarely invade the soma (Watanabe *et al.* 2006). This inability of the waves to invade the soma was attributed to dilution of IP_3 as it diffused from the dendrite into the soma. In confirmation of this, synaptically evoked waves could be made to invade the soma by increasing basal levels of IP_3 either directly via the patch pipette, or by bath application of low concentrations of carbachol (Watanabe *et al.* 2006). These contrasting results may be explained by differences in physiology of the BLA and the hippocampus. The hippocampus is a layered structure and the synaptic stimulation protocols would be focus stimulation and probably generate IP_3 on a small portion of the dendritic tree. In this instance IP_3 would diffuse from a single location becoming increasing diluted as it reached the soma. The amygdala is not a layered structure and it is likely that our synaptic stimulation protocols stimulate metabotropic receptors and generate IP_3 at a variety of locations throughout the neuron and possibly even the soma itself (e.g. Fig. 1*D*). Thus, the relative ease with which we were able to evoke Ca^{2+} waves that invade the soma and nucleus is likely to be due to the a more diffuse production of IP_3. The strong and distributed cholinergic innervation of these neurons would further enhance this propagation.

In the absence of metabotropic receptor stimulation, AP-evoked Ca^{2+} rises are highest in thin dendrites, with only very small rises being recorded in the soma and nucleus. As neurons in the basolateral complex are largely silent *in vivo* (Paré *et al.* 1995), and APs produce only a very small rise in nuclear Ca^{2+}, it is unlikely that Ca^{2+} entry through voltage-gated Ca^{2+} channels activated by APs has much effect on nuclear Ca^{2+} signalling. In contrast, metabotropic receptor stimulation via activation of IP_3-sensitive Ca^{2+} stores is able to produce large sustained rises in nuclear Ca^{2+}. Perhaps most important is the ability of APs and coincident metabotropic receptor activation to act synergistically to produce a large nuclear Ca^{2+} response. The nuclear envelope has extensive Ca^{2+} stores and can release Ca^{2+} via IP_3 receptors (Stehno-Bittel *et al.* 1995). While our results are consistent with diffusion of Ca^{2+} from the soma into the nucleus, it is also possible that the nuclear Ca^{2+} signal observed during IP_3-CICR is due to release of Ca^{2+} from the nuclear envelope.

Our data show (Figs 1*E* and 4*C*) that increasing metabotropic stimulation and presumably IP_3 increases the extent of wave propagation. Thus, the concentration of IP_3 is a critical factor in determining wave propagation. From the data shown in Fig. 9 it appears that Ca^{2+} influx during APs helps waves propagate into the nucleus, suggesting that the Ca^{2+} also plays role in determining the spatial extent of wave propagation in the soma and nucleus. This result appears surprising as one may expect that once the waves are initiated, store-released Ca^{2+} should be able to supply the Ca^{2+} to maintain propagation, observed in CA1 pyramidal neurons (Watanabe *et al.* 2006). There are two possible explanations for our results in Fig. 9. First, IP_3 receptors may have a clustered distribution, and diffusion of Ca^{2+} is tightly regulated so that the concentration of Ca^{2+} reaching the next cluster may fail to produce a fully regenerative response. Second, as discussed above, as the BLA is not a layered structure, our stimulation protocol would activate synapses that are distributed through the neuron and IP_3 levels may not be uniformly elevated in all instances. Ca^{2+} from APs may facilitate propagation through regions of low levels of IP_3. Perhaps, the Ca^{2+} from APs may not be extending the waves, but initiating the Ca^{2+} release at somatic and possibly even nuclear IP_3 receptors.

A multitude of biochemical events in neurons is initiated by rises in cytosolic Ca^{2+} (Berridge *et al.* 2000). Activation of voltage-dependent Ca^{2+} channels that open during the AP leads to rapid and large rises of Ca^{2+} throughout the dendritic tree (Markram *et al.* 1995). However, these Ca^{2+} rises have a fast onset and decay, whereas many Ca^{2+}-dependent processes have slower rate constants of activation (Ross *et al.* 2005). In contrast, Ca^{2+} release from intracellular stores leads to larger rises in Ca^{2+}, has slower kinetics, and acts to amplify AP-evoked Ca^{2+} rises. Thus, this may be a mechanism to modulate Ca^{2+}-dependent processes that APs cannot drive in isolation.

Functional implications

The prevailing cellular model of classical conditioning in the amygdala is that coincident activation of conditioned stimuli (CS) and unconditioned stimuli (US) inputs to neurons in the BLA leads to the induction of synaptic plasticity of CS inputs (LeDoux, 2000; Davis & Whalen, 2001). In this model, NMDA receptors act as the coincidence detectors. The depolarization from US afferents relieves the Mg^{2+} block of NMDA receptors present at synapses made by CS afferents, causing Ca^{2+} influx through the NMDA receptors and triggering biochemical changes that result in potentiation of the CS afferents. However, NMDA receptors are not the only point of coincidence detection in BLA neurons. Associative learning in the amygdala also involves metabotropic glutamate receptor activation. Supra-linear Ca^{2+} rises are induced by coincident metabotropic stimulation and APs (IP_3-CICR; Fig. 9), as well as coincident mGluR and AChR activation (Fig. 3). As store content and release potential are dependent on prior neuronal activity (Power & Sah, 2005), the Ca^{2+} signal also conveys information about prior activity. This IP_3-mediated store release is not observed in the distal spine-dense dendrites, where most excitatory synaptic contacts are made, but is instead restricted to proximal compartments including the nucleus. It has long been proposed that IP_3-mediated store release may link synaptic activity to changes in gene transcription (Berridge, 1998). While it is possible that AP signals on their own can affect nuclear signalling (Mermelstein *et al.* 2000), store release (Dolmetsch *et al.* 1998; Li *et al.* 1998; Hardingham *et al.* 2001) as well as rises in nuclear Ca^{2+} (Hardingham *et al.* 2001) have been shown to be effective in initiating gene transcription. Glutamatergic synapses within the BLA have a key role in amygdala-related learning (LeDoux, 2000; Davis & Whalen, 2001; Sah *et al.* 2003). The activity of the cholinergic system is enhanced during behavioural states, such as attention and emotional arousal, and muscarinic activity is critical for the learning and consolidation of numerous behavioural paradigm (Pepeu & Giovannini, 2004). Our data suggest that cooperative action of the glutamatergic and cholinergic systems in controlling nuclear Ca^{2+} signalling may be one mechanism by which these two systems interact in BLA-associated memory storage.

References

Barbara JG (2002). IP_3-dependent calcium-induced calcium release mediates bidirectional calcium waves in neurones: functional implications for synaptic plasticity. *Biochim Biophys Acta* **1600**, 12–18.

Ben-Ari Y, Zigmond RE, Shute CC & Lewis PR (1977). Regional distribution of choline acetyltransferase and acetylcholinesterase within the amygdaloid complex and stria terminalis system. *Brain Res* **120**, 435–444.

Berridge MJ (1998). Neuronal calcium signaling. *Neuron* **21**, 13–26.

Berridge MJ, Lipp P & Bootman MD (2000). The versatility and universality of calcium signalling. *Nat Rev Mol Cell Biol* **1**, 11–21.

Bezprozvanny I, Watras J & Ehrlich BE (1991). Bell-shaped calcium-response curves of Ins(1,4,5)P3- and calcium-gated channels from endoplasmic reticulum of cerebellum. *Nature* **351**, 751–754.

Bootman MD, Berridge MJ & Roderick HL (2002*a*). Calcium signalling: more messengers, more channels, more complexity. *Curr Biol* **12**, R563–R565.

Bootman MD, Collins TJ, Mackenzie L, Roderick HL, Berridge MJ & Peppiatt CM (2002*b*). 2-Aminoethoxydiphenyl borate (2-APB) is a reliable blocker of store-operated Ca^{2+} entry but an inconsistent inhibitor of InsP3-induced Ca^{2+} release. *FASEB J* **16**, 1145–1150.

Carlsen J & Heimer L (1986). A correlated light and electron microscopic immunocytochemical study of cholinergic terminals and neurons in the rat amygdaloid body with special emphasis on the basolateral amygdaloid nucleus. *J Comp Neurol* **244**, 121–136.

Carlsen J, Zaborszky L & Heimer L (1985). Cholinergic projections from the basal forebrain to the basolateral amygdaloid complex: a combined retrograde fluorescent and immunohistochemical study. *J Comp Neurol* **234**, 155–167.

Caulfield MP (1993). Muscarinic receptors – characterization, coupling and function. *Pharmacol Ther* **58**, 319–379.

Connor JA (1993). Intracellular calcium mobilization by inositol 1,4,5-trisphosphate: intracellular movements and compartmentalization. *Cell Calcium* **14**, 185–200.

Davis M & Whalen PJ (2001). The amygdala: vigilance and emotion. *Mol Psychiatry* **6**, 13–34.

Dolmetsch RE, Xu K & Lewis RS (1998). Calcium oscillations increase the efficiency and specificity of gene expression. *Nature* **392**, 933–936.

Elston GN & DeFelipe J (2002). Spine distribution in cortical pyramidal cells: a common organizational principle across species. *Prog Brain Res* **136**, 109–133.

Faber ES & Sah P (2002). Physiological role of calcium-activated potassium currents in the rat lateral amygdala. *J Neurosci* **22**, 1618–1628.

Faber ES, Sedlak P, Vidovic M & Sah P (2006). Synaptic activation of transient receptor potential channels by metabotropic glutamate receptors in the lateral amygdala. *Neuroscience* **137**, 781–794.

Fendt M & Schmid S (2002). Metabotropic glutamate receptors are involved in amygdaloid plasticity. *Eur J Neurosci* **15**, 1535–1541.

Finch EA & Augustine GJ (1998). Local calcium signalling by inositol-1,4,5-trisphosphate in Purkinje cell dendrites. *Nature* **396**, 753–756.

Finch EA, Turner TJ & Goldin SM (1991). Calcium as a coagonist of inositol 1,4,5-trisphosphate-induced calcium release. *Science* **252**, 443–446.

Fiorillo CD & Williams JT (1998). Glutamate mediates an inhibitory postsynaptic potential in dopamine neurons. *Nature* **394**, 78–82.

Fitzjohn SM & Collingridge GL (2002). Calcium stores and synaptic plasticity. *Cell Calcium* **32**, 405–411.

Gasparini F, Lingenhohl K, Stoehr N, Flor PJ, Heinrich M, Vranesic I, Biollaz M, Allgeier H, Heckendorn R, Urwyler S, Varney MA, Johnson EC, Hess SD, Rao SP, Sacaan AI, Santori EM, Velicelebi G & Kuhn R (1999). 2-Methyl-6-(phenylethynyl)-pyridine (MPEP), a potent, selective and systemically active mGlu5 receptor antagonist. *Neuropharmacology* **38**, 1493–1503.

Gulledge AT & Stuart GJ (2005). Cholinergic inhibition of neocortical pyramidal neurons. *J Neurosci* **25**, 10308–10320.

Hardingham GE, Arnold FJ & Bading H (2001). Nuclear calcium signaling controls CREB-mediated gene expression triggered by synaptic activity. *Nat Neurosci* **4**, 261–267.

Himpens B, De Smedt H & Casteels R (1994). Relationship between [Ca^{2+}] changes in nucleus and cytosol. *Cell Calcium* **16**, 239–246.

Horowitz SB & Moore LC (1974). The nuclear permeability, intracellular distribution, and diffusion of inulin in the amphibian oocyte. *J Cell Biol* **60**, 405–415.

Humeau Y, Herry C, Kemp N, Shaban H, Fourcaudot E, Bissiere S & Luthi A (2005). Dendritic spine heterogeneity determines afferent-specific Hebbian plasticity in the amygdala. *Neuron* **45**, 119–131.

Ichikawa T & Hirata Y (1986). Organization of choline acetyltransferase-containing structures in the forebrain of the rat. *J Neurosci* **6**, 281–292.

Iino M (1990). Biphasic Ca^{2+} dependence of inositol 1,4,5-trisphosphate-induced Ca^{2+} release in smooth muscle cells of the guinea pig taenia caeci. *J Gen Physiol* **95**, 1103–1122.

Jacob SN, Choe CU, Uhlen P, DeGray B, Yeckel MF & Ehrlich BE (2005). Signaling microdomains regulate inositol 1,4,5-trisphosphate-mediated intracellular calcium transients in cultured neurons. *J Neurosci* **25**, 2853–2864.

Jaffe DB & Brown TH (1994). Metabotropic glutamate receptor activation induces calcium waves within hippocampal dendrites. *J Neurophysiol* **72**, 471–474.

Kapur A, Yeckel M & Johnston D (2001). Hippocampal mossy fiber activity evokes Ca^{2+} release in CA3 pyramidal neurons via a metabotropic glutamate receptor pathway. *Neuroscience* **107**, 59–69.

Larkum ME, Watanabe S, Nakamura T, Lasser-Ross N & Ross WN (2003). Synaptically activated Ca^{2+} waves in layer 2/3 and layer 5 rat neocortical pyramidal neurons. *J Physiol* **549**, 471–488.

LeDoux JE (2000). Emotion circuits in the brain. *Annu Rev Neurosci* **23**, 155–184.

Li W, Llopis J, Whitney M, Zlokarnik G & Tsien RY (1998). Cell-permeant caged InsP3 ester shows that Ca^{2+} spike frequency can optimize gene expression. *Nature* **392**, 936–941.

Li R, Nishijo H, Wang Q, Uwano T, Tamura R, Ohtani O & Ono T (2001). Light and electron microscopic study of cholinergic and noradrenergic elements in the basolateral nucleus of the rat amygdala: evidence for interactions between the two systems. *J Comp Neurol* **439**, 411–425.

Lujan R, Roberts JD, Shigemoto R, Ohishi H & Somogyi P (1997). Differential plasma membrane distribution of metabotropic glutamate receptors mGluR1 alpha, mGluR2 and mGluR5, relative to neurotransmitter release sites. *J Chem Neuroanat* **13**, 219–241.

McDonald AJ (1982). Neurons of the lateral and basolateral amygdaloid nuclei: a golgi study in the rat. *J Comp Neurol* **212**, 293–312.

McDonald AJ (1992). Projection neurons of the basolateral amygdala: a correlative Golgi and retrograde tract tracing study. *Brain Res Bull* **28**, 179–185.

McGaugh JL (2004). The amygdala modulates the consolidation of memories of emotionally arousing experiences. *Annu Rev Neurosci* **27**, 1–28.

Mak DO, McBride S & Foskett JK (1998). Inositol 1,4,5-trisphosphate [correction of tris-phosphate] activation of inositol trisphosphate [correction of tris-phosphate] receptor Ca^{2+} channel by ligand tuning of Ca^{2+} inhibition. *Proc Natl Acad Sci U S A* **95**, 15821–15825.

Maravall M, Mainen ZF, Sabatini BL & Svoboda K (2000). Estimating intracellular calcium concentrations and buffering without wavelength ratioing. *Biophys J* **78**, 2655–2667.

Marino MJ, Rouse ST, Levey AI, Potter LT & Conn PJ (1998). Activation of the genetically defined m1 muscarinic receptor potentiates *N*-methyl-D-aspartate (NMDA) receptor currents in hippocampal pyramidal cells. *Proc Natl Acad Sci U S A* **95**, 11465–11470.

Markram H, Helm PJ & Sakmann B (1995). Dendritic calcium transients evoked by single back-propagating action potentials in rat neocortical pyramidal neurons. *J Physiol* **485**, 1–20.

Maruyama T, Kanaji T, Nakade S, Kanno T & Mikoshiba K (1997). 2APB, 2-aminoethoxydiphenyl borate, a membrane-penetrable modulator of Ins(1,4,5)P3-induced Ca^{2+} release. *J Biochem (Tokyo)* **122**, 498–505.

Mash DC & Potter LT (1986). Autoradiographic localization of M1 and M2 muscarine receptors in the rat brain. *Neuroscience* **19**, 551–564.

Mermelstein PG, Bito H, Deisseroth K & Tsien RW (2000). Critical dependence of cAMP response element-binding protein phosphorylation on L-type calcium channels supports a selective response to EPSPs in preference to action potentials. *J Neurosci* **20**, 266–273.

Mesulam MM, Mufson EJ, Wainer BH & Levey AI (1983). Central cholinergic pathways in the rat: an overview based on an alternative nomenclature (Ch1–Ch6). *Neuroscience* **10**, 1185–1201.

Morikawa H, Khodakhah K & Williams JT (2003). Two intracellular pathways mediate metabotropic glutamate receptor-induced Ca^{2+} mobilization in dopamine neurons. *J Neurosci* **23**, 149–157.

Mrzljak L, Levey AI & Goldman-Rakic PS (1993). Association of m1 and m2 muscarinic receptor proteins with asymmetric synapses in the primate cerebral cortex: morphological evidence for cholinergic modulation of excitatory neurotransmission. *Proc Natl Acad Sci U S A* **90**, 5194–5198.

Nagai T, Kimura H, Maeda T, McGeer PL, Peng F & McGeer EG (1982). Cholinergic projections from the basal forebrain of rat to the amygdala. *J Neurosci* **2**, 513–520.

Nakamura T, Barbara JG, Nakamura K & Ross WN (1999). Synergistic release of Ca^{2+} from IP_3-sensitive stores evoked by synaptic activation of mGluRs paired with backpropagating action potentials. *Neuron* **24**, 727–737.

Nakamura T, Lasser-Ross N, Nakamura K & Ross WN (2002). Spatial segregation and interaction of calcium signalling mechanisms in rat hippocampal CA1 pyramidal neurons. *J Physiol* **543**, 465–480.

Nakamura T, Nakamura K, Lasser-Ross N, Barbara JG, Sandler VM & Ross WN (2000). Inositol 1,4,5-trisphosphate (IP_3)-mediated Ca^{2+} release evoked by metabotropic agonists and backpropagating action potentials in hippocampal CA1 pyramidal neurons. *J Neurosci* **20**, 8365–8376.

O'Malley DM (1994). Calcium permeability of the neuronal nuclear envelope: evaluation using confocal volumes and intracellular perfusion. *J Neurosci* **14**, 5741–5758.

Paré D, Pape HC & Dong J (1995). Bursting and oscillating neurons of the cat basolateral amygdaloid complex *in vivo*: electrophysiological properties and morphological features. *J Neurophysiol* **74**, 1179–1191.

Parekh AB & Putney JW Jr (2005). Store-operated calcium channels. *Physiol Rev* **85**, 757–810.

Pepeu G & Giovannini MG (2004). Changes in acetylcholine extracellular levels during cognitive processes. *Learn Mem* **11**, 21–27.

Peppiatt CM, Collins TJ, Mackenzie L, Conway SJ, Holmes AB, Bootman MD, Berridge MJ, Seo JT & Roderick HL (2003). 2-Aminoethoxydiphenyl borate (2-APB) antagonises inositol 1,4,5-trisphosphate-induced calcium release, inhibits calcium pumps and has a use-dependent and slowly reversible action on store-operated calcium entry channels. *Cell Calcium* **34**, 97–108.

Power AE, McIntyre CK, Litmanovich A & McGaugh JL (2003). Cholinergic modulation of memory in the basolateral amygdala involves activation of both m1 and m2 receptors. *Behav Pharmacol* **14**, 207–213.

Power JM & Sah P (2002). Nuclear calcium signaling evoked by cholinergic stimulation in hippocampal CA1 pyramidal neurons. *J Neurosci* **22**, 3454–3462.

Power JM & Sah P (2005). Intracellular calcium store filling by an L-type calcium current in the basolateral amygdala at subthreshold membrane potentials. *J Physiol* **562**, 439–453.

Power JM & Sah P (2006). Enhancement of the AHP and spike frequency adaptation by acetylcholine in projection neurons of the basolateral amygdala: program No. 342.15 *Abstract Viewer and Itinerary Planner. Washington, DC: Soc Neurosci*. Online.

Pozzo-Miller LD, Petrozzino JJ, Golarai G & Connor JA (1996). Ca^{2+} release from intracellular stores induced by afferent stimulation of CA3 pyramidal neurons in hippocampal slices. *J Neurophysiol* **76**, 554–562.

Rainnie DG & Shinnick-Gallagher P (1992). Trans-ACPD and L-APB presynaptically inhibit excitatory glutamatergic transmission in the basolateral amygdala (BLA). *Neurosci Lett* **139**, 87–91.

Ramsey IS, Delling M & Clapham DE (2006). An introduction to TRP channels. *Annu Rev Physiol* **68**, 619–647.

Rodrigues SM, Bauer EP, Farb CR, Schafe GE & LeDoux JE (2002). The group I metabotropic glutamate receptor mGluR5 is required for fear memory formation and long-term potentiation in the lateral amygdala. *J Neurosci* **22**, 5219–5229.

Ross WN, Nakamura T, Watanabe S, Larkum M & Lasser-Ross N (2005). Synaptically activated Ca^{2+} release from internal stores in CNS neurons. *Cell Mol Neurobiol* **25**, 283–295.

Sah P & Clements JD (1999). Photolytic manipulation of $[Ca^{2+}]_i$ reveals slow kinetics of potassium channels underlying the afterhyperpolarization in hippocampal pyramidal neurons. *J Neurosci* **19**, 3657–3664.

Sah P, Faber ES, Lopez De Armentia M & Power J (2003). The amygdaloid complex: anatomy and physiology. *Physiol Rev* **83**, 803–834.

Stehno-Bittel L, Luckhoff A & Clapham DE (1995). Calcium release from the nucleus by InsP3 receptor channels. *Neuron* **14**, 163–167.

Takechi H, Eilers J & Konnerth A (1998). A new class of synaptic response involving calcium release in dendritic spines. *Nature* **396**, 757–760.

Taylor CW & Marshall IC (1992). Calcium and inositol 1,4,5-trisphosphate receptors: a complex relationship. *Trends Biochem Sci* **17**, 403–407.

Tinsley MR, Quinn JJ & Fanselow MS (2004). The role of muscarinic and nicotinic cholinergic neurotransmission in aversive conditioning: comparing pavlovian fear conditioning and inhibitory avoidance. *Learn Mem* **11**, 35–42.

Washburn MS & Moises HC (1992*a*). Electrophysiological and morphological properties of rat basolateral amygdaloid neurons in vitro. *J Neurosci* **12**, 4066–4079.

Washburn MS & Moises HC (1992*b*). Muscarinic responses of rat basolateral amygdaloid neurons recorded in vitro. *J Physiol* **449**, 121–154.

Watanabe S, Hong M, Lasser-Ross N & Ross WN (2006). Modulation of calcium wave propagation in the dendrites and to the soma of rat hippocampal pyramidal neurons. *J Physiol* **575**, 455–468.

Watanabe Y, Ikegaya Y, Saito H & Abe K (1995). Roles of $GABA_A$, NMDA and muscarinic receptors in induction of long-term potentiation in the medial and lateral amygdala in vitro. *Neurosci Res* **21**, 317–322.

Womble MD & Moises HC (1992). Muscarinic inhibition of M-current and a potassium leak conductance in neurones of the rat basolateral amygdala. *J Physiol* **457**, 93–114.

Womble MD & Moises HC (1993). Muscarinic modulation of conductances underlying the afterhyperpolarization in neurons of the rat basolateral amygdala. *Brain Res* **621**, 87–96.

Womble MD & Moises HC (1994). Metabotropic glutamate receptor agonist ACPD inhibits some, but not all, muscarinic-sensitive K^+ conductances in basolateral amygdaloid neurons. *Synapse* **17**, 69–75.

Yajeya J, De La Fuente Juan A, Bajo VM, Riolobos AS, Heredia M & Criado JM (1999). Muscarinic activation of a non-selective cationic conductance in pyramidal neurons in rat basolateral amygdala. *Neuroscience* **88**, 159–167.

Yamada S, Takechi H, Kanchiku I, Kita T & Kato N (2004). Small-conductance Ca^{2+}-dependent K^+ channels are the target of spike-induced Ca^{2+} release in a feedback regulation of pyramidal cell excitability. *J Neurophysiol* **91**, 2322–2329.

Yasuda R, Nimchinsky EA, Scheuss V, Pologruto TA, Oertner TG, Sabatini BL & Svoboda K (2004). Imaging calcium concentration dynamics in small neuronal compartments. *Sci STKE* **2004**, pl5.

Acknowledgements

This work was supported by grants from the National Health and Medical Research Council of Australia and the Australian Research Council. J.P. is a recipient of a Smart State Fellowship from the Queensland State Government.

Supplemental material

The online version of this paper can be accessed at:
DOI: 10.1113/jphysiol.2006.125062
http://jp.physoc.org/cgi/content/full/jphysiol.2006.125062/DC1
and contains supplemental material consisting of a figure:

Supplemental Figure 1. Comparison of somatic and nuclear fluorescent responses

This material can also be found as part of the full-text HTML version available from http://www.blackwell-synergy.com